Acta Applicandae Mathematicae **11** (1988), 49–96

Low-Order Spectral Models of the Atmospheric Circulation: A Survey

H. E. DE SWART
*Centre for Mathematics and Computer Science, P.O. Box 4079, 1009 AB Amsterdam, The Netherlands**

(Received: 26 June 1987)

Abstract. A quasi-geostrophic potential vorticity equation is derived from the Navier–Stokes equations for atmospheric motions. It describes the evolution of a quasi-horizontally flow on time scales of a few days and more. The associated boundary-value problem is analyzed by projection of the equation onto orthonormal eigenfunctions (modes) of a Sturm–Liouville operator. The result is a spectral model, consisting of an infinite number of nonlinear ordinary differential equations for the evolution of the mode amplitudes. Low-order spectral models, in which only a few modes are resolved, appear to have properties which agree with observations of the atmospheric circulation. However, little justification is available for truncating the spectral expansion at low resolution numbers. It is argued that stochastic forcing terms should be added to the equations, but it is not a priori clear how they should be specified.

A derivation is presented of a specific low-order spectral model of the quasi-geostrophic potential vorticity equation. Some of its subsystems are analyzed for their physical and mathematical properties. It appears that topography can act as a triggering mechanism to generate multiple equilibria. The corresponding flow patterns resemble preference states of the atmospheric circulation. The systems can vacillate between three characteristic regimes with transitions provided either by external or internal mechanisms. A discussion is presented on the validity of stochastically forced spectral models and deterministic chaotic models for the atmospheric circulation.

AMS subject classifications (1980). 86A10, 76E20, 35A35, 34C35.

Key words and phrases. Interaction between planetary waves and synoptic eddies, low-order models, bifurcation analysis, vacillation between weather regimes.

1. Introduction

1.1. VARIABILITY OF THE PLANETARY WAVES

Weather conditions have a significant influence on daily life. Consequently, there is great public interest in understanding the atmospheric circulation and in forecasting the weather. Although the qualitative dynamics of the circulation are nowadays rather well understood, forecasting has remained a cumbersome task. For example, it appears that results of numerical weather prediction models have significance for at most two weeks. It is known that this fact is due to the intrinsic

*Present affiliation: Institute of Meteorology and Oceanography, Princetonplein 5, 3584 CC, Utrecht, The Netherlands.

finite predictability of the atmosphere. In order to understand this fundamental property, we have to consider the dynamics of the circulation.

Basically, the driving mechanism is the inhomogeneous radiation input of the sun, which causes a heat surplus in the tropical areas and a heat deficit near the poles. These differences create a meridional temperature gradient in the midlatitudes, giving rise to slopes of the pressure levels, thereby forcing the air to move polewards. However, globally a balance will be established with the Coriolis force, resulting in quasi-horizontally westerly winds. This so-called geostrophic balance applies to a flow outside the frictional boundary layer, which is situated near the earth's surface.

From a daily weather-map it can immediately be seen that this flow is not zonally symmetric; it has a wavelike structure in which several length scales are present. In the first place we have the planetary waves, with a typical length scale of 10 000 km. These semi-permanent structures are forced by the thermal differences between land and oceans and by the large-scale topographic variations (called the orography). It appears that this flow is unstable: small perturbations may increase their amplitudes, in this way withdrawing energy from the basic flow. These disturbances, called transient eddies, appear on the weather-map as high- and low-pressure cells. They have a typical length scale of 1000 km and their life (a few days) is much shorter than that of the planetary waves (a few weeks). The positions of the eddies are rather unpredictable.

Model studies have demonstrated that the geographical distribution of the planetary waves largely determines the development of the transient eddies, see Frederiksen (1983). There is also an opposite effect, as argued by Opsteegh and Vernekar (1982), i.e., the transient eddies are capable of forcing and altering the planetary waves. The nonlinear interactions between different scales of motion cause the atmosphere to have a limited predictability (Lorenz, 1969, 1984).

Obviously, it is not possible to predict the actual flow state of the atmosphere over a large time interval with a sufficiently large probability. Therefore, it becomes worthwhile to distinguish between weather regimes, i.e., clusters of states representing nearly the same flow pattern. This was done, for instance, by Baur *et al.* (1944). They published a catalogue of large-scale atmospheric circulation patterns over Central Europe, which they called *Grosswetterlagen*. Later on, Hess and Brezowsky (1969) classified these weather regimes into three categories. These are a zonal (high index) regime with strong westerlies and small wave amplitudes, a meridional (low index) regime with large waves embedded in a weak zonal flow and a transitional regime. The observed vacillation between the various regimes, known to synoptic meterologists for a long time (Namias, 1950), is due to the interactions between the quasi-stationary planetary waves and the transient eddies. Little is known about these transitions corresponding to breaks in the weather, see Oerlemans (1978). Within the framework of long-term weather forecasting, it is important to obtain a better understanding of the dynamics responsible for this vacillation behaviour.

Basically this problem should be analyzed from the full equations of motion, but they are too complicated to handle analytically. However, they describe motions on all length and time scales, while we are only interested in time scales of at least a few days and length scales of the order 1000 km and more. In Section 2.1 these assumptions are used to reduce the equations of motion to a single nonlinear partial differential equation. It is called the quasi-geostrophic potential vorticity equation, being the starting-point of many studies on large-scale atmospheric flow. It describes the evolution of a quantity called the stream-function, to which all state variables governing the motion (velocities, temperature, pressure and density) are related.

1.2. THE USE OF SPECTRAL MODELS

The quasi-geostrophic potential vorticity equation is nonlinear, consequently it is difficult to analyze. One way to deal with this problem is to expand the solution in a series of eigenfunctions (modes) of an associated Sturm–Liouville problem. Projecting the partial differential equation on these eigenfunctions, we obtain a dynamical system of the type

$$\dot{\Psi} = f_{\mu}(\Psi), \tag{1.1}$$

where the dot denotes differentiation with respect to time. It consists of an infinite number of coupled ordinary differential equations describing the time evolution of the mode amplitudes represented by the vector Ψ. Here $f_{\mu}(\Psi)$ is a vector field depending on parameters $\mu = (\mu_1, \mu_2, \ldots)$. Details of the spectral technique are considered in the Sections 2.2 and 2.3. A discussion is included about the work of Constantin *et al.* (1985) on the relevance of truncated spectral models in which only a finite number of modes are considered. In most cases the truncation number must be large in order to obtain agreement between the approximate and exact solution.

In recent years, many low-order spectral models of the quasi-geostrophic potential vorticity equation have been studied. The basic motivation was to investigate in what sense they reflect properties of the large-scale atmospheric circulation. The frequent references to papers on spectral models are an indication for the importance of spectral theory in modern dynamic meteorology. Extensive references are presented in Section 3.1. Next, in Section 3.2 a derivation of a low-order spectral model of a two-level version of the quasi-geostrophic potential vorticity equation in a beta plane channel geometry is given. This includes the barotropic model of Charney and DeVore (1979) and the baroclinic models of Charney and Straus (1980) and Reinhold and Pierrehumbert (1982).

From a mathematical point of view, truncated spectral models can be analyzed with techniques originating from dynamical systems theory, see Guckenheimer and Holmes (1983) and Thompson and Stewart (1986). The structure of the

vector fields studied in this paper is such that small-volume elements in phase space always shrink and that solutions are bounded. Consequently, for $t \to \infty$ trajectories tend to bounded sets of limit points with zero volume in phase space. These may include regular sets such as stationary points (corresponding to equilibrium flow patterns), limit cycles (oscillating flow) and invariant tori (quasi-periodically oscillating flow), as well as strange attractors (irregular, chaotic flow). We wish to determine these sets of limit points. The spectral model mimics a typical characteristic of the atmospheric circulation if trajectories irregularly vacillate between different preferent regions in phase space. Therefore, we are particularly interested in the occurrence of multiple unstable regular solutions and strange attractors. We expect trajectories to wander on a strange attractor and to visit alternately regions in phase space close to the regular solutions. If on the other hand the system tends to a regular limit set, the truncation is apparently to severe. Thus, more modes should be included in order to obtain a better representation. Another possibility is to add stochastic perturbations to the spectral equations. They account for the effect of small-scale eddies on the dynamics of the long waves. In this case the dynamics will be fundamentally different and the analysis requires application of the theory of stochastic processes. In the Sections 4 and 5 a few low-dimensional spectral models are studied. The existence of multiple equilibria and strange attractors is investigated by means of a bifurcation analysis. Since there are many free parameters in the model, it is necessary to use physical arguments in order to uncover its essential features.

Multiple equilibria can be generated either by topography or thermal asymmetries. The corresponding flow patterns resemble quasi-stationary preference states of the atmospheric circulation. It appears that all models can vacillate between three weather regimes, which are of zonal, meridional, and mixed type. The latter is necessarily visited if the zonal or meridional regime is left, with a possibility for the system returning to the original regime. This is very similar to the Grosswetterlagen dynamics described previously. Vacillation is generated either internally, due to the chaotic dynamics, or provided by external, stochastic sources. A discussion about the validity of low-order spectral models to describe large-scale atmospheric flow is presented in the final section.

2. A Quasi-Geostrophic Model: Method of Analysis

2.1. DERIVATION OF A POTENTIAL VORTICITY EQUATION

The state of the dry atmospheric circulation is specified by a three-dimensional velocity vector $\mathbf{u}$, density ρ, pressure p and temperature T. Consequently six equations are needed to describe its dynamics. They are obtained from the momentum, mass and heat balances of the fluid, see Gill (1982). The results are

$$\frac{d\mathbf{u}}{dt} + 2\boldsymbol{\Omega} \times \mathbf{u} = -\frac{1}{\rho} \nabla p + \mathbf{g} + \mathbf{F}_w, \qquad \frac{d\rho}{dt} + \rho \nabla \cdot \mathbf{u} = 0, \qquad p = \rho RT,$$
$$\frac{d\theta}{dt} = \frac{\theta}{c_p T} H^*. \tag{2.1}$$

Here t is time, ∇ the nabla operator, $\boldsymbol{\Omega}$ the rotation vector of the earth, $\mathbf{g}$ the acceleration of gravity, $\mathbf{F}_w$ are frictional forces per unit mass and R is the gas constant for dry air. Furthermore,

$$\theta = T\left(\frac{p^*}{p}\right)^{R/c_p} \tag{2.2}$$

is the potential temperature, with $p*$ a reference pressure and c_p the heat capacity of air at constant pressure. Finally H^* is a heating function. Both $\mathbf{F}_w$ and H^* will be specified later. System (2.1) consists of three momentum equations, a continuity equation, an equation of state (the ideal gas law) and a thermodynamic heat equation, respectively.

To analyze Equations (2.1) we need *a-priori* knowledge of the type of motion to be considered. The geometry of the earth suggests to develop the equations in spherical coordinates λ, ϕ and r, which are longitude, latitude and distance to the centre of the earth respectively, see Figure 1. The resulting equations can be found in Pedlosky (1979). We will consider an atmospheric flow at midlatitudes, which is characterized by a small aspect ratio δ and a small Rossby number ϵ. Here

$$\delta = lH, \qquad \epsilon = \frac{\sigma}{f_0}, \quad f_0 = 2\Omega \sin \phi_0, \tag{2.3}$$

with l^{-1} and H a horizontal and vertical length scale of the flow respectively, σ^{-1} a time scale and f_0 (the Coriolis parameter) the vertical component of the rotation vector at some central latitude $\phi = \phi_0$. This implies that the flow is

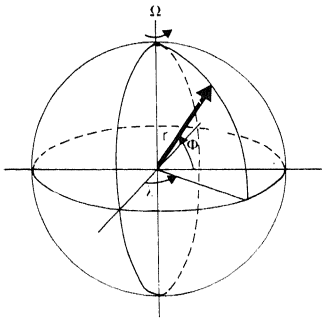

Fig. 1. Spherical coordinates for the earth.

quasi-horizontal (approximately parallel to the earth's surface) and that it has a time scale which is much larger than the typical rotation period of the earth.

In the state of rest ($\mathbf{u} = 0$) the momentum equations reduce to the hydrostatic balance

$$\frac{\mathrm{d}p_s(r)}{\mathrm{d}r} = -\rho_s(r)\, g. \tag{2.4}$$

In principle any density profile can be chosen, as long as

$$\frac{\mathrm{d}\theta_s}{\mathrm{d}r} \geqslant 0, \quad \theta_s(r) = \frac{p^*}{R\rho_s}\left(\frac{p_s}{p^*}\right)^{1-R/c_p}. \tag{2.5}$$

It means that the potential temperature θ_s, calculated from (2.1) and (2.2), nowhere decreases with height. This condition implies that we are dealing with a stably stratified fluid (Gill, 1982). Next, nondimensional variables, denoted by primes, are introduced as follows (Pedlosky, 1979):

$$\begin{aligned}
&r_0\left(\cos\phi_0 \frac{\mathrm{d}\lambda}{\mathrm{d}t}, \frac{\mathrm{d}\phi}{\mathrm{d}t}\right) = \sigma l^{-1}(u', v'), && \frac{\mathrm{d}r}{\mathrm{d}t} = \delta\sigma l^{-1} w', \\
&\lambda = (lr_0 \cos\phi_0)^{-1} x', && \phi = \phi_0 + (lr_0)^{-1} y', \\
&r = r_0 + Hz', && t = \sigma^{-1} t', \\
&p = p_s + \rho_s f_0 \sigma l^{-2} p', && H^* = c_p T f_0 \sigma^2 (gHl^2)^{-1} H^{*\prime}, \\
&\rho = \rho_s\{1 + \epsilon F\alpha^2 \rho'\}, && \theta = \theta_s\{1 + \epsilon F\alpha^2 \theta'\}.
\end{aligned} \tag{2.6}$$

Here u', v' and w' are the nondimensional zonal, meridional and vertical velocity component, respectively. The parameter r_0 is the radius of the earth and

$$\alpha = (lr_0)^{-1}, \qquad F = \frac{f_0^2 r_0^2}{gH}. \tag{2.7}$$

We will take α to be a small parameter, which indicates that the uniform horizontal length-scale is small compared to the radius of the earth. The parameter F, measuring the squared ratio of the earth's radius and the external Rossby radius, is of order unity for this type of flow.

Next we expand u', v', w', p', ρ' and θ' in the small parameters δ, ϵ and α. After dropping the primes, we find that the zeroth-order approximations of the state variables (denoted by the subscript 0) can be related to one variable Ψ, called the streamfunction. The relations are

$$\begin{aligned}
&u_0 = -\frac{\partial\Psi}{\partial y}, \qquad v_0 = \frac{\partial\Psi}{\partial x}, \qquad w_0 = 0, \\
&p_0 = \Psi, \qquad \rho_0 = -\frac{\Psi}{\rho_s}\frac{\mathrm{d}\rho_s}{\mathrm{d}z}, \qquad \theta_0 = \frac{\partial\Psi}{\partial z}.
\end{aligned} \tag{2.8}$$

A closed system of dynamic equations is obtained by considering the zeroth-order vertical vorticity balance, following from cross-differentiation of the

horizontal momentum equations, and the thermodynamic equation. Using (2.8) the result is

$$\frac{d_0}{dt}(\nabla_h^2\Psi + f) = \frac{1}{\rho_s}\frac{\partial}{\partial z}(\rho_s w_1), \tag{2.9a}$$

$$\frac{d_0}{dt}\frac{\partial\Psi}{\partial z} + w_1 S = H^*. \tag{2.9b}$$

Here w_1 is the first-order vertical velocity and

$$\nabla_h = \left(\frac{\partial}{\partial x}, \frac{\partial}{\partial y}\right), \qquad \frac{d_0}{dt} = \frac{\partial}{\partial t} - \frac{\partial\Psi}{\partial y}\frac{\partial}{\partial x} + \frac{\partial\Psi}{\partial x}\frac{\partial}{\partial y}. \tag{2.10}$$

Furthermore

$$f = \frac{2\Omega}{\sigma}\sin\phi_0 + \beta y, \quad \beta = \frac{2\Omega\cos\phi_0}{\sigma l r_0}, \qquad S(z) = \frac{(\alpha^2 F)^{-1}}{\theta_s}\frac{\partial\theta_s}{\partial z} \geqslant 0, \tag{2.11}$$

where the condition $S(z) \geqslant 0$ is a consequence of (2.5). The lower and upper boundary conditions to (2.9) can be formulated as (Pedlosky, 1979)

$$\int_0^1 \frac{1}{\rho_s}\frac{\partial}{\partial z}(\rho_s w_1)\,dz = \underbrace{-\gamma\frac{d_0 h}{dt}}_{(1)} \underbrace{- C\nabla_h^2\Psi(z=0)}_{(2)} + \underbrace{C\nabla_h^2\psi^*}_{(3)}, \tag{2.12}$$

where

$$\gamma = \frac{f_0 h_0}{\sigma H}, \qquad C = \frac{f_0\delta_E}{2\sigma H}. \tag{2.13}$$

They describe the modification of the flow at the lower boundary due to the presence of topography (1), frictional effects (2) and due to an external forcing streamfunction ψ^*(3). Here $z = h$ describes the position of the lower boundary having a characteristic amplitude $h_0 (\ll H)$. Furthermore, δ_E is the thickness of the frictional boundary layer situated at the lower boundary.

Eliminating w_1 in (2.9a) and (2.12) with (2.9b) we obtain

$$\frac{d_0}{dt}\left[\nabla_h^2\Psi + \frac{1}{\rho_s}\frac{\partial}{\partial z}\left(\frac{\rho_s}{S}\frac{\partial\Psi}{\partial z}\right) + f\right] = \frac{1}{\rho_s}\frac{\partial}{\partial z}\left(\frac{\rho_s H^*}{S}\right), \tag{2.14a}$$

$$\int_0^1 \frac{1}{\rho_s}\frac{\partial}{\partial z}\left[\frac{\rho_s}{S}\left(H^* - \frac{d_0}{dt}\frac{\partial\Psi}{\partial z}\right)\right]dz = -\gamma\frac{d_0 h}{dt} - C\nabla_h^2\Psi(z=0) + C\nabla_h^2\psi^*. \tag{2.14b}$$

Hence, we have reduced the full equations of motion to one nonlinear partial differential equation for the streamfunction Ψ. In the absence of heating ($H^* = 0$) it expresses conservation of the quantity

$$q = \nabla_h^2\Psi + \frac{1}{\rho_s}\frac{\partial}{\partial z}\left(\frac{\rho_s}{S}\frac{\partial\Psi}{\partial z}\right) + f. \tag{2.15}$$

This constant of motion is the quasi-geostrophic potential vorticity. Here $\nabla_h^2\Psi$ is the relative vorticity. The specification quasi-geostrophic is added because Equation (2.14a) models a flow which is approximately in a geostrophic balance. This balance slowly varies due to the presence of small vertical velocities.

In the limit $S \to 0$ and $H^* = 0$ (constant potential temperature θ_s and no heating) it follows from (2.9b) that if Ψ is independent of z initially, it will for all t be a z-independent function ψ. Integrating (2.9a) over the vertical and using the boundary conditions (2.12), we obtain

$$\frac{d_0}{dt}[\nabla_h^2\psi + \gamma h + f] = -C\nabla_h^2(\psi - \psi^*), \tag{2.16}$$

which is the barotropic potential vorticity equation.

In some papers the quasi-geostrophic Equations (2.9a, b), (2.14a) or (2.16) are considered with $f = (2\Omega/\sigma)\sin\phi$. Furthermore, an additional contribution $-\alpha^2 F\psi$ may be present between the brackets on the left-hand side of (2.16). This Cressman correction term describes the production of vorticity due to variations in the free surface of the fluid. In particular, the long waves, for which $\alpha^2 F = \mathcal{O}(1)$, are affected by this mechanism. However, we recall that the quasi-geostrophic equations hold, providing that the parameter δ, ϵ and α are small. Consequently, the quasi-geostrophic model has a restricted validity: it is not valid over the entire sphere and it does not describe the planetary wave dynamics. Nevertheless, in many studies it is used as a simplified model of the large-scale atmospheric circulation.

2.2. VERTICAL RESOLUTION: LEVEL MODELS

We consider the partial differential equation (2.14a) on a domain with appropriate boundary conditions. It is analyzed by expanding the solution Ψ in a series of eigenfunctions $\{e_j\}_j$ of an associated Sturm–Liouville operator:

$$\Psi = \sum_j \Psi_j e_j;\ j = (j_1, j_2, \ldots, j_d), \tag{2.17}$$

where d is the dimension of the domain, see Gottlieb and Orszag (1977) and Voigt *et al.* (1984). In this case $d = 3$ and the Sturm–Liouville problem is obtained from (2.14a) by looking at the eigenfunctions of the vorticity field:

$$\nabla_h^2 e_j + \frac{1}{\rho_s}\frac{\partial}{\partial z}\left(\frac{\rho_s}{S}\frac{\partial}{\partial z}e_j\right) + \lambda_j^2 e_j = 0. \tag{2.18}$$

The eigenfunctions have positive eigenvalues λ_j^2, satisfy the boundary conditions and are orthonormalized with respect to the domain average. Projecting (2.14a) on these eigenfunctions (Galerkin projection) we obtain a dynamical system of the type (1.1). It describes the time evolution of the expansion coefficients $\{\Psi_j(t)\}_j = \boldsymbol{\Psi}$.

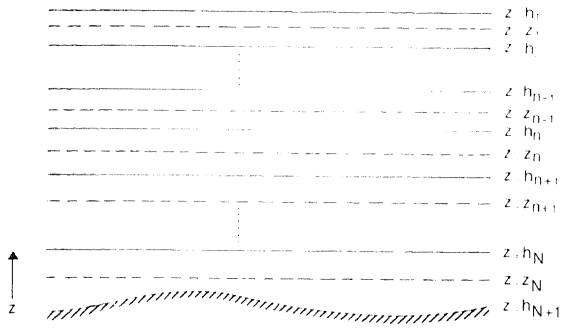

Fig. 2. Level model for a continuously stratified fluid Equation (2.9a) is considered on the levels $z = z_n$ and Equation (2.9b) on $z = h_n$ ($n = 1, 2, \ldots, N$).

Using the properties of the eigenfunctions (completeness) Dutton (1974) has shown that the solution (2.17) of (2.14a) on a bounded domain exists and is unique. In a subsequent paper (Dutton, 1976a) general properties of the spectral equations and its solutions are discussed. In order to construct the spectral model equations, the eigenfunctions must be specified. As can be seen from (2.14b) the vertical boundary conditions generally are too complicated to calculate the eigenfunctions analytically. Since the horizontal boundary conditions are often chosen rather elementary (for example, periodic) this problem can be dealt with the following way. First Equation (2.14a) is discretized in the vertical (Pedlosky, 1979): starting from Equations (2.9a, b), the vorticity equation is evaluated at a finite number of levels $z = z_1, z = z_2, \ldots, z = z_N$. In a similar manner, the thermodynamic equations are derived at the intermediate levels $z = h_1$, $z = h_2, \ldots, z = h_{N+1}$, see Figure 2. Derivatives in the vertical are approximated by central difference schemes.

The result is a set of N partial differential equations for the streamfunctions $\{\psi(z_n)\}_{n=1}^{N}$:

$$\frac{\mathrm{d}_0}{\mathrm{d}t}[\nabla_h^2\Psi(z_n)+f] = -F_n^{(1)}\frac{\mathrm{d}_0}{\mathrm{d}t}[\Psi(z_{n-1})-\Psi(z_n)]+ \tag{2.19}$$

$$+F_n^{(2)}\frac{\mathrm{d}_0}{\mathrm{d}t}[\Psi(z_n)-\Psi(z_{n+1})]+F_n^{(3)}, \quad n = 1, 2, \ldots, N.$$

Here $F_n^{(1)}$, $F_n^{(2)}$ and $F_n^{(3)}$ are parameters which depend on the stratification and heating profiles. As shown by Pedlosky (1979), the introduction of a finite level version of Equation (2.14a) can be seen as a discretization of the continuous stratification of the fluid. This implies that, although the finite level version (2.19) of (2.14a) can only describe approximate solutions, it represents the dynamics of a real physical system.

2.3. TRUNCATION AT A HORIZONTAL LEVEL

We now apply the spectral method to the set of Equations (2.19). We have the expansions

$$\Psi(z_n) = \sum_{\mathbf{j}} \Psi_{\mathbf{j}}(z_n)\phi_{\mathbf{j}}, \tag{2.20}$$

where the $\{\phi_{\mathbf{j}}\}_{\mathbf{j}}$ are orthogonal eigenfunctions of the two-dimensional Laplace operator:

$$\nabla_h^2\phi_{\mathbf{j}} + \lambda_{\mathbf{j}}^2\phi_{\mathbf{j}} = 0, \quad \mathbf{j} = (j_1, j_2), \tag{2.21}$$

subject to the boundary conditions. Assuming that (2.21) can be solved analytically, we can derive the spectral equations for the expansion coefficients $\Psi_j(z_n)$. They are again a system of the type (1.1).

We should consider an infinite-dimensional phase space, which cannot be realized in practical applications. A convenient way to deal with this problem in fluid dynamics is to approximate the solutions (2.20) by expansions in which $\mathbf{j}$ may run only through a finite number (say K) of values:

$$\tilde{\Psi}(z_n) = \sum_{\mathbf{j}} \Psi_{\mathbf{j}}(z_n)\phi_{\mathbf{j}}, \quad \mathbf{j}_l \leqslant \mathbf{j} \leqslant \mathbf{j}_u. \tag{2.22}$$

Projecting the N partial differential equations on these eigenfunctions, we obtain a finite-dimensional system:

$$\dot{\boldsymbol{\Psi}} = f_{\mu}(\boldsymbol{\Psi}) + \mathbf{F}(t) \quad \text{in } \mathbb{R}^M, \quad M = KN. \tag{2.23}$$

The forcing terms $\mathbf{F}(t)$ represent the effect of the unresolved modes on the resolved modes and additional physical processes not incorporated in the model. In many studies they are *a priori* put equal to zero. A justification for doing this is found in the observation that generally most energy is contained in only a few modes (the long waves). From a more formal point of view Constantin *et al.* (1985) have studied the problem for the full Navier–Stokes equations. They found that for large times a finite mode expansion could be selected such that qualitative agreement is obtained with the exact solution, in the sense that they have equal stability and attractor properties. Furthermore, they showed that

$$M_s \geqslant (lL_D)^{-d} \tag{2.24}$$

is a sufficient condition for the truncation number in order to obtain such qualitative agreement. Here L_D is a dissipation length scale and d the dimension of the flow. Generally M_s will be a large number, but we remark that (2.24) is not a necessary condition. The numerical results of Franceschini *et al.* (1984) with a truncated spectral model of the Navier–Stokes equations in two dimensions indicate a stabilization of qualitative behaviour at $M \sim 100$. Although it is not yet clear whether these results are applicable to the quasi-geostrophic potential

vorticity equation, they at least suggest that it is useful to study truncated spectral models.

For small truncation numbers it is not allowed to neglect the effect of the forcing terms in (2.23). In some studies this is compensated for by choosing stochastic forcing with a parametrization of its statistical moments. From a theoretical point of view, this choice is difficult to justify. One of the few results obtained so far can be found in Kottalam *et al.* (1987). They state that the forcing terms have indeed a stochastic nature but their moments are very complicated. We will return to this point later on.

3. Spectral Models of the Atmospheric Circulation

3.1. A REVIEW OF THE LITERATURE

The fact that Galerkin projection techniques can be applied to the partial differential equations describing the dynamics of large-scale atmospheric flow was first realized by Silberman (1954). In this paper a one-level, i.e., barotropic, version of Equations (2.9) is considered without the effects of forcing, dissipation and topography. The streamfunction is expanded in orthonormal eigenfunctions of the Laplace operator on the sphere, being spherical harmonics. A similar model for a two-level version of (2.9) in spherical geometry was developed by Bryan (1959).

It is remarked that the spectral method applied to Equations (2.9) is actually invalid on the sphere, because it is not allowed that the meridional length-scale becomes of the same order as the radius of the earth. For this reason Saltzman (1959) introduced a channel approximation, in which the equations are considered in a circular strip at midlatitudes, see Figure 3. However, this approach requires artificial boundary conditions at the two walls.

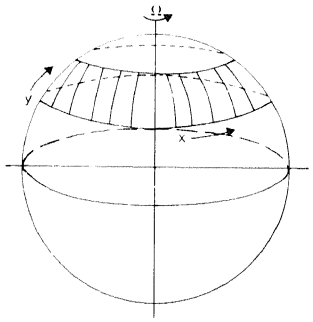

Fig. 3. The midlatitude channel. The x-coordinate is along lines of constant latitude, the y-coordinate along lines of constant longitude.

In the first instance the spectral technique was mainly used to solve low-order models either analytically or numerically. At the time people became interested in the spectral method as an alternative for the grid-point method to numerically solve nonlinear partial differential equations. For the quasi-geostrophic model experiments were already carried out by Kubota *et al.* (1961). Their conclusion is that spectral methods give better results than grid-point models. On the other hand, the spectral scheme turns out to be rather inefficient, because the inclusion of many eigenfunctions requires the storage of a large number of interaction coefficients. Consequently, computations are time and storage consuming and thus expensive. As an alternative Orszag (1970) developed a transform method. Instead of projecting the nonlinear terms directly on the spectral components, the Jacobians are evaluated at grid points each time step and next transformed to the spectral components. This scheme appears to be fast and accurate and is therefore applied in many numerical weather forecasting models, such as the one of the European Centre for Medium-range Weather Forecasting (ECMWF) in Reading, England (Jarraud and Baede, 1985). After the introduction of the transform method, the direct interaction method has been mainly used as an analytical tool to study low-order models.

Table I. List of references to relevant studies on deterministic low-order spectral models of one and two level versions of the potential vorticity equation (2.14a) in different geometries

One level, spherical	One level, channel
Silberman (1954)	Saltzman (1959)
Kubota (1961)	Lorenz (1960)
Platzman (1962)	Lilly (1965)
Baer (1970)	Vickroy and Dutton (1979)
Baer (1971)	Charney and DeVore (1979)
Dutton (1976b)	Lorenz (1980)
Wiin Nielsen (1979)	Mitchell and Dutton (1981)
Källén (1981)	Shirer and Wells (1983)
Källén (1982)	De Swart (1987a)
Wiin Nielsen (1984)	De Swart (1987b)
Legras and Ghil (1985)	
Two levels, spherical	**Two levels, channel**
Bryan (1959)	Lorenz (1963b)
Baer (1970)	Lorenz (1965)
Baer (1971)	Yao (1980)
Galin (1979)	Charney and Straus (1980)
Källén (1983)	Roads (1980)
Galin and Kirchkov (1985)	Reinhold and Pierrehumbert (1982)
	Yoden (1983a)
	Yoden (1983b)

Forcing and dissipation mechanisms in barotropic spectral models of the atmospheric circulation with a spherical geometry have been introduced by Wiin-Nielsen (1979). For the case of a beta plane these mechanisms have been analyzed by Vickroy and Dutton (1979). The combined effect of forcing, dissipation and topography has first been studied by Charney and DeVore (1979) for a beta plane channel geometry. A spherical analogon was discussed by Källen (1981). These studies demonstrate that forced systems may have multiple equilibria for a range of parameter values and the associated flow patterns resemble large-scale preference states of the atmospheric circulation. Similar models have been considered in many papers, see Table I for references. Models with additional nongeostrophic effects have been analyzed by Lorenz (1980, 1984).

A first, numerical study on the effects of topography in a two-level spectral model was presented by Yao (1980). This was followed by the analytical studies of Charney and Straus (1980), Roads (1980) and, for a spherical geometry, that of Källén (1983). Low-order spectral models of multi-level versions of the quasi-geostrophic equation are discussed in Roads (1982) and Yoden and Mukougawa (1983). Spectral models including humidity effects can be found in Lorenz (1982).

3.2. A TWO-LEVEL MODEL IN A BETA PLANE CHANNEL

Up to now mainly one- and two-level versions of the quasi-geostrophic potential vorticity equation have been studied analytically. The two-level reads

$$\frac{d_0}{dt}[\nabla_h^2\Psi(z_1)+f] = F'\frac{d_0}{dt}[\Psi(z_1)-\Psi(z_2)] - F'(z_1-z_2)H^*(h_2) + \\ - C'\nabla_h^2[\Psi(z_1)-\Psi(z_2)] \tag{3.1a}$$

$$\frac{d_0}{dt}[\nabla_h^2\Psi(z_2)+f] = -F'\frac{d_0}{dt}[\Psi(z_1)-\Psi(z_2)] + F'(z_1-z_2)H^*(h_2) + \\ + C'\nabla_h^2[\Psi(z_1)-\Psi(z_2)] - 2\left[\gamma\frac{d_0 h}{dt} + C\nabla_h^2(\Psi(z_2)-\psi^*)\right], \tag{3.1b}$$

where

$$F' = [S(h_2)(z_1-z_2)^2]^{-1}. \tag{3.2}$$

The contributions involving the coefficient C' model the internal friction at the boundary level $z = h_2$ between the two layers. Next we introduce

$$\psi = \tfrac{1}{2}[\Psi(z_1)+\Psi(z_2)], \qquad \tau = \tfrac{1}{2}[\Psi(z_1)-\Psi(z_2)], \tag{3.3}$$

which are the barotropic and baroclinic streamfunction, respectively. Note that τ is proportional to the potential temperature. The heating at $z = h_2$ is parametrized as

$$H^*(h_2) = \frac{a}{z_1 - z_2}(\tau^* - \tau), \tag{3.4}$$

where a^{-1} is a nondimensional thermal relaxation time and τ^* is the baroclinic thermal forcing. The damping is a crude representation of the cooling due to infrared outgoing radiation. The equations for ψ and τ read

$$\frac{\partial}{\partial t}\nabla_h^2\psi + J(\psi, \nabla_h^2\psi) + J(\tau, \nabla_h^2\tau) + \gamma J(\psi - \tau, h) + J(\psi, f)$$
$$= -C\nabla_h^2(\psi - \psi^* - \tau), \tag{3.5a}$$

$$\frac{\partial}{\partial t}\nabla_h^2\tau + J(\psi, \nabla_h^2\tau) + J(\tau, \nabla_h^2\psi) - \gamma J(\psi - \tau, h) + J(\tau, f)$$
$$= F'\left[\frac{\partial\tau}{\partial t} + J(\psi, \tau)\right] + C\nabla_h^2(\psi - \psi^* - \tau) - aF'(\tau^* - \tau) - 2C'\nabla_h^2\tau, \tag{3.5b}$$

where

$$J(A, B) = (\mathbf{e}_z \times \nabla_h A) \cdot \nabla_h B \tag{3.6}$$

is the Jacobian of A and B with $\mathbf{e}_z$ a unity vector in the z-direction. The vertical velocity at the midlevel $z = h_z$ satisfies

$$w_1(h_2) = F'\left\{a(\tau^* - \tau) - \frac{\partial\tau}{\partial t} - J(\psi, \tau)\right\}. \tag{3.7}$$

We now apply the spectral method to (3.5). Thus, on a domain with boundary conditions, we expand ψ, ψ^*, τ, τ^* and h in the eigenfunctions defined in (2.21). The resulting spectral equations are presented in Appendix A. Next we must specify the eigenfunctions. To this end we take the domain to be a rectangular channel on a beta plane, with length $2\pi/b$ in the x-direction and width π in the y-direction. In fact this is the midlatitude channel shown in Figure 3. Here

$$b = \frac{2B}{L}, \tag{3.8}$$

with B and L the dimensional width and length of the channel. We investigate the existence of travelling wave solutions in the x-direction. At the boundaries $y = 0$ and $y = B$ the meridional velocity is zero. Furthermore, no circulation may develop at the boundaries. The resulting conditions for the streamfunction are derived by Phillips (1954). They lead to the following eigenvalue problem:

$$\nabla_h^2\phi_j + \lambda_j^2\phi_j = 0 \text{ on } \{(x, y) \mid 0 \leq x \leq 2\pi/b,\ 0 \leq y \leq \pi\},$$
$$\phi_j\left(x + \frac{2\pi}{b}\right) = \phi_j(x),$$
$$\frac{\partial\phi_j}{\partial x} = 0 \quad \text{and} \quad \int_0^{2\pi/b} \frac{\partial\phi_j}{\partial y}\,dx = 0 \text{ at } y = 0 \text{ and } y = \pi, \tag{3.9}$$

$$\langle \phi_{\mathbf{j}}, \phi_{\mathbf{l}} \rangle \equiv \frac{b}{2\pi^2} \int_0^{\pi} \int_0^{2\pi/b} \phi_{\mathbf{j}} \phi_{\mathbf{l}}^{cc} \, \mathrm{d}x \, \mathrm{d}y = \delta_{\mathbf{jl}}.$$

Here cc denotes a complex conjugate and $\delta_{\mathbf{jl}}$ a Kronecker delta function. It can easily be verified that the following eigenfunctions, with associated eigenvalues, obey (3.9):

$$\phi_{\mathbf{j}}(y) = \sqrt{2} \cos(j_2 y); \qquad \lambda_{\mathbf{j}}^2 = j_2^2, \tag{3.10a}$$

$$\phi_{\mathbf{j}}(x, y) = \sqrt{2}\, \mathrm{e}^{ij_1 bx} \sin(j_2 y); \quad \lambda_{\mathbf{j}}^2 = j_1^2 b^2 + j_2^2, \tag{3.10b}$$

$$j_1 = \pm 1, \pm 2, \ldots; \quad j_2 = 1, 2, \ldots$$

The eigenfunctions in (3.10a) are $(0, j_2)$ modes, which describe purely zonal flows. The solutions in (3.10b) are $(|j_1|, j_2)$ wave modes. With this information we can calculate the interaction coefficients defined in (A3) of Appendix A. The results are presented in Appendix B. It appears that the nonlinearities always occur as triads, with the interaction of two modes affecting the evolution of a third one. This is due to the fact that the basic equations of fluid mechanics only contain quadratic nonlinearities. As shown in Appendix B, many of these interactions are forbidden. The underlying physical mechanism is discussed in Pedlosky (1979).

We now present a particular low-order model by including only the (0, 1), (0, 2), (1, 1), (1, 2), (2, 1) and (2, 2) modes. These are two zonal flow profiles and four planetary waves, respectively. We assume that external forcing only acts upon the zonal flow modes. They model a zonal flow forcing due to the equator-pole temperature gradient. Furthermore

$$h = \cos(bx) \sin(y), \tag{3.11}$$

i.e., the topography is given as a (1, 1) mode, being the longest wave present in the model.

Defining the real variables

$$\begin{aligned}
&x_1 = \psi_{01}, && x_1^* = \psi_{01}^*, && y_1 = \tau_{01}, && y_1^* = \tau_{01}^*, \\
&x_2 = \frac{1}{\sqrt{2}}(\psi_{11} + \psi_{-11}), && x_3 = \frac{i}{\sqrt{2}}(\psi_{11} - \psi_{-11}), && y_2 = \frac{1}{\sqrt{2}}(\tau_{11} + \tau_{-11}), && y_3 = \frac{i}{\sqrt{2}}(\tau_{11} - \tau_{-11}), \\
&x_4 = \psi_{02}, && x_4^* = \psi_{02}^*, && y_4 = \tau_{02}, && y_4^* = \tau_{02}^*, \\
&x_5 = \frac{1}{\sqrt{2}}(\psi_{12} + \psi_{-12}), && x_6 = \frac{i}{\sqrt{2}}(\psi_{12} - \psi_{-12}), && y_5 = \frac{1}{\sqrt{2}}(\tau_{12} + \tau_{-12}), && y_6 = \frac{i}{\sqrt{2}}(\tau_{12} - \tau_{-12}), \\
&x_7 = \frac{1}{\sqrt{2}}(\psi_{21} + \psi_{-21}), && x_8 = \frac{i}{\sqrt{2}}(\psi_{21} - \psi_{-21}), && y_7 = \frac{1}{\sqrt{2}}(\tau_{21} + \tau_{-21}), && y_8 = \frac{i}{\sqrt{2}}(\tau_{21} - \tau_{-21}), \\
&x_9 = \frac{1}{\sqrt{2}}(\psi_{22} + \psi_{-22}), && x_{10} = \frac{i}{\sqrt{2}}(\psi_{22} - \psi_{-22}), && y_9 = \frac{1}{\sqrt{2}}(\tau_{22} + \tau_{-22}), && y_{10} = \frac{i}{\sqrt{2}}(\tau_{22} - \tau_{-22}),
\end{aligned} \tag{3.12}$$

we arrive at the twenty component model given in Appendix C. This is the basic model to be studied in this paper. Note that it is an example of a dissipative dynamical system, see Guckenheimer and Holmes (1983). Consequently, volume elements in phase space always shrink and solutions are bounded. Thus, for $t \to \infty$ trajectories in phase space tend to a bounded set of limit points of zero volume in phase space. We are in particular interested in the nontransient behaviour of the system, i.e., once it has settled down to its attractor.

In papers published so far, channels at the central latitude $\phi_0 = 45°$ have been considered, which makes $f_0 = 1.10^{-4}\,s^{-1}$ and $\beta_0 = 1.6\ 10^{-11}\,m^{-1}\,s^{-1}$. The vertical length-scale will be fixed at $H = 10$ km and the time scale at $\sigma^{-1} = 10^5$ s, which is about one day. The thermal relaxation time is varied between two and 10 days ($0.5 \geqslant a \geqslant 0.1$), the topographic amplitude between 0 and 4 km ($0 \leqslant \gamma \leqslant 4$), dissipation time scales between two days and two weeks ($0.5 \geqslant C,\ C' \geqslant 0.07$) and the stratification parameter $(F')^{-1}$ between 0 and 0.2. In the next two sections we will study low-order barotropic and baroclinic models which are special cases of the 20 component model mentioned above. We will stay within the specified range of parameter values.

4. Barotropic Models

4.1. PRELIMINARIES

Consider the 20 component model of Appendix C for the case of a constant potential temperature of the fluid ($F' \to \infty$, equivalently $\sigma_0 \to 0$). Furthermore, let baroclinic forcing mechanisms be absent ($y_1^* = y_4^* = 0$). If the baroclinic y-components are taken zero initially, they remain zero for all times and solutions are governed by the 10 coefficient barotropic model

$$
\begin{aligned}
\dot{x}_1 &= \gamma_{11}^* x_3 - C(x_1 - x_1^*),\\
\dot{x}_2 &= -(\alpha_{11}x_1 - \beta_{11})x_3 - Cx_2 - \delta_{11}x_4x_6 - \rho_{11}(x_5x_8 - x_6x_7),\\
\dot{x}_3 &= (\alpha_{11}x_1 - \beta_{11})x_2 - \gamma_{11}x_1 - Cx_3 + \delta_{11}x_4x_5 + \rho_{11}(x_5x_7 + x_6x_8),\\
\dot{x}_4 &= \gamma_{12}^* x_6 - C(x_4 - x_4^*) + \epsilon_1(x_2x_6 - x_3x_5) + \epsilon_2(x_7x_{10} - x_8x_9),\\
\dot{x}_5 &= -(\alpha_{12}x_1 - \beta_{12})x_6 - Cx_5 - \delta_{12}x_3x_4 + \rho_{12}(x_2x_8 - x_3x_7) + \gamma'_{12}x_8,\\
\dot{x}_6 &= (\alpha_{12}x_1 - \beta_{12})x_5 - \gamma_{12}x_4 - Cx_6 + \delta_{12}x_2x_4 - \rho_{12}(x_2x_7 + x_3x_8) - \gamma'_{12}x_7,\\
\dot{x}_7 &= -(\alpha_{21}x_1 - \beta_{21})x_8 - Cx_7 - \delta_{21}x_4x_{10} - \rho_{21}(x_2x_6 + x_3x_5) + \gamma'_{21}x_6,\\
\dot{x}_8 &= (\alpha_{21}x_1 - \beta_{21})x_7 - Cx_8 + \delta_{21}x_4x_9 + \rho_{21}(x_2x_5 - x_3x_6) - \gamma'_{21}x_5,\\
\dot{x}_9 &= -(\alpha_{22}x_1 - \beta_{22})x_{10} - Cx_9 - \delta_{22}x_4x_8,\\
\dot{x}_{10} &= (\alpha_{22}x_1 - \beta_{22})x_9 - Cx_{10} + \delta_{22}x_4x_7\,.
\end{aligned}
\tag{4.1}
$$

The coefficients α_{nm}, β_{nm}, γ_{nm}, γ_{nm}^*, γ'_{nm}, δ_{nm}, ϵ_n and ρ_{nm} depend on the model

parameters b, γ and β, see Appendix C. Furthermore,

$$\sqrt{x_1^{*2} + 4x_4^{*2}} = \frac{Ul}{\sigma} \tag{4.2}$$

is a driving Rossby number of the flow with U a typical velocity scale of the external forcing. Equations (4.1) are in fact a low-order model of the barotropic potential vorticity Equation (2.16). They are invariant under the transformation

$$\begin{aligned}&(x_1, x_2, x_3, x_4, x_5, x_6, x_7, x_8, x_9, x_{10}, x_1^*, x_4^*) \rightarrow \\ &\quad \rightarrow (x_1, x_2, x_3, -x_4, -x_5, -x_6, -x_7, -x_8, x_9, x_{10}, x_1^*, -x_4^*).\end{aligned} \tag{4.3}$$

The system contains a six-dimensional subsystem, as indicated by the dashed lines. For $x_4^* = 0$ it is further reduced to the three-dimensional system between the dotted lines. The latter will be analyzed in the next subsection, the six-component model is considered in Section 4.3 and we return to the 10 component model in Section 4.4.

4.2. THREE COMPONENTS

The three-component model in (4.1) between the dotted lines is the simplest nontrivial spectral model of the large-scale atmospheric circulation. It describes the interaction between a zonal flow and a planetary wave mode. To study the properties of the nonlinearities explicitly, we first neglect the effect of forcing and dissipation ($x_1^* = C = 0$). The stationary points $\hat{x} = (\hat{x}_1, \hat{x}_2, \hat{x}_3)$ of this model, obtained by setting all time derivatives equal to zero, satisfy

$$\hat{x}_2 = \frac{\gamma_{11}\hat{x}_1}{\alpha_{11}\hat{x}_1 - \beta_{11}}, \qquad \hat{x}_3 = 0, \tag{4.4}$$

for arbitrary $\hat{x}_1$. Since $\hat{x}_3 = 0$ the wave is in phase with the topography. To investigate the stability of the equilibria we consider the dynamics of small perturbations on these states. They evolve as $\exp(\lambda t)$, where λ are the eigenvalues of the Jacobian matrix of the vector field, linearized at $\hat{x}$. In this case the characteristic equation reads

$$\lambda\left[\lambda^2 + (\alpha_{11}\hat{x}_1 - \beta_{11})^2 - \frac{\gamma_{11}\gamma_{11}^*\beta_{11}}{\alpha_{11}\hat{x}_1 - \beta_{11}}\right] = 0. \tag{4.5}$$

A stationary point is unstable if there is at least one eigenvalue with a positive real part. In (4.5) this is the case if

$$0 < \alpha_{11}\hat{x}_1 - \beta_{11} < (\gamma_{11}\gamma_{11}^*\beta_{11})^{1/3}. \tag{4.6}$$

Note that instabilities can only occur for γ nonzero. For this reason the mechanism is called topographic instability (Charney and DeVore, 1979). In the limit $(\alpha_{11}\hat{x}_1 - \beta_{11}) \rightarrow 0$ the wave amplitude grows resonantly. This is due to a

continuous vorticity transfer from the topography to the wave (the mountain torque) which cannot be compensated for by vorticity advection.

Next we introduce zonal forcing and dissipation. Then stationary points are found from a cubic equation:

$$\hat{x}_1^3 + a_2\hat{x}_1^2 + a_1\hat{x}_1 + a_0 = 0, \qquad \hat{x}_2 = \frac{\gamma_{11}\hat{x}_1(\alpha_{11}\hat{x}_1 - \beta_{11})}{(\alpha_{11}\hat{x}_{11} - \beta_{11})^2 + C^2},$$

$$\hat{x}_3 = \frac{-C\gamma_{11}\hat{x}_1}{(\alpha_{11}\hat{x}_1 - \beta_{11})^2 + C^2}, \tag{4.7}$$

where

$$a_2 = \frac{-(2\beta_{11} + \alpha_{11}x_1^*)}{\alpha_{11}}, \qquad a_1 = \frac{2\alpha_{11}\beta_{11}x_1^* + \beta_{11}^2 + \gamma_{11}\gamma_{11}^* + C^2}{\alpha_{11}^2},$$

$$a_0 = \frac{-(\beta_{11}^2 + C^2)x_1^*}{\alpha_{11}^2}. \tag{4.8}$$

It can easily be shown that $0 < \hat{x}_1 \leq x_1^*$. Thus $\hat{x}_3 < 0$, which implies that the phase difference between the stationary wave and the topography is always negative. As can be seen from (4.7), due to dissipation the topographic resonance has shifted to small but nonzero values of $(\alpha_{11}\hat{x}_1 - \beta_{11})$. According to (4.7), there may be one or three real stationary points. The bifurcation set, which is the set of parameter values at which a transition from one to three equilibria occurs, is given by

$$q^3 + r^2 = 0, \quad q = \tfrac{1}{3}a_1 - \tfrac{1}{9}a_2^2, \; r = \tfrac{1}{6}(a_1a_2 - 3a_0) - \tfrac{1}{27}a_2^3. \tag{4.9}$$

The stationary points at the bifurcation set are limit points (turning points) of the bifurcation diagram. For these parameter values the wave becomes topographically unstable. In the region where $(q^3 + r^2)$ is negative, called the catastrophe set, three real stationary points occur.

The stability is determined from the eigenvalues of the Jacobian matrix of the vector field linearized at $\hat{x}$. The characteristic equation reads

$$(\lambda + C)^3 + b_1(\lambda + C) + b_0 = 0,$$

$$b_1 = (\alpha_{11}\hat{x}_1 - \beta_{11})^2 - \gamma_{11}\gamma_{11}^*\left[\frac{\beta_{11}(\alpha_{11}\hat{x}_1 - \beta_{11}) - C^2}{(\alpha_{11}\hat{x}_1 - \beta_{11})^2 + C^2}\right], \tag{4.10}$$

$$b_0 = \frac{-C\gamma_{11}\gamma_{11}^*\alpha_{11}\hat{x}_1(\alpha_{11}\hat{x}_1 - \beta_{11})}{(\alpha_{11}\hat{x}_1 - \beta_{11})^2 + C^2}.$$

From (4.7) and (4.10) it follows that if the system has only one real stationary point it is stable. If there are three real stationary points, two of them are stable and one is unstable. Furthermore, it can be shown that complex eigenvalues cannot have vanishing real parts, hence there are no Hopf bifurcation points. The only possibility for a real eigenvalue to pass through zero is at the bifurcation set.

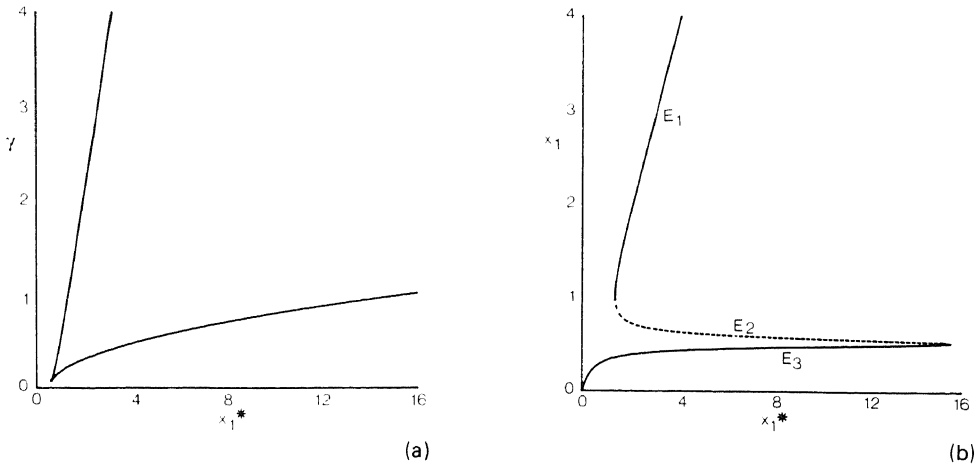

Fig. 4. (a) Bifurcation set in the γ, x_1^*-parameter space of the three component model. (b) Steady solution component $\hat{x}_1$ as a function of x_1^* for $\gamma = 1$. A solid line denotes that the solution is stable, a dashed line denotes an unstable solution.

As a specific example we fix the parameter values at $b = 2$, $C = 0.1$ and $\beta = 2.5$. They are similar to those of Charney and DeVore (1979), except that we have a time scale σ^{-1} of 10^5 s instead of 10^4 s. The domain is a channel, centered at the latitude $\phi_0 = 45°$, with length and width equal to 5000 km. The zonal wavelength is 5000 km and a dissipation time scale of 10 days is taken. In the literature, the model has also been studied for different parameter values, see Table I for references. The results of these investigations do not differ significantly from those which will be presented here. In Figure 4a the bifurcation set of the model in the γ, x_1^*-parameter space, enclosing the catastrophe set, is shown. It is known as a cusp catastrophe. In Figure 4b the equilibrium solution component $\hat{x}_1$, which represents the nondimensional intensity of the zonal flow, is presented as a function of the external forcing x_1^* ($= U/U_0$, where $U_0 = 15.91\ \mathrm{ms}^{-1}$) for $\gamma = 1$ (i.e., a topography amplitude of 1 km). For large x_1^* (≥ 15.566) there is one stable stationary point E_1. For smaller forcing values ($1.336 \leq x_1^* \leq 15.566$) two more stationary points appear. The intermediate one (E_2) is unstable: it has one positive real eigenvalue, while the lower one (E_3) is stable. For small x_1^* (≤ 1.336) one stable stationary point (E_3) is left. Characteristic flow patterns associated with the equilibria E_1, E_2, and E_3 are shown in Figure 5. E_1 represents a high index state with a strong westerly flow and a small wave amplitude. E_3 is a low index state with a large wave embedded in a weak zonal flow. Finally E_2 is an intermediate state.

In Figure 6 a projection of trajectories onto the $x_1 - x_2$ plane is shown for the case of three real stationary points. Initial conditions are taken in a plane $x_3 = \text{constant}$. It appears that generally trajectories tend to one of the stable equilibria. Exceptions are those which lie on the separatrix between the attraction

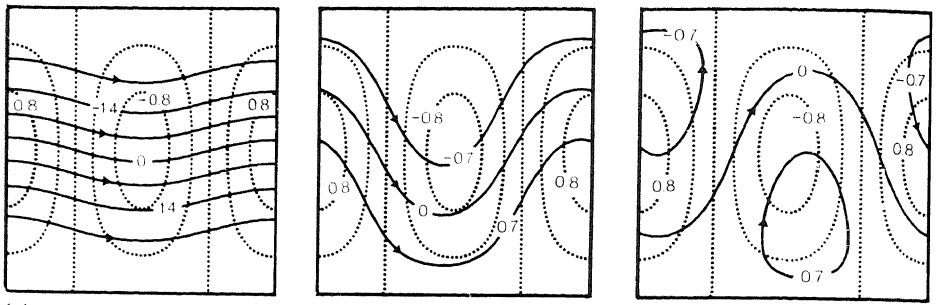

Fig. 5. Nondimensional streamfunction patterns of the equilibria $E_1(a)$, $E_2(b)$ and $E_3(c)$ for $\gamma = 1$, $x_3^* = 2$. $\Delta\psi = 1$ corresponds to a zonal transport of $2.6 \times 10^7 \, m^2 s^{-1}$. The dashed lines represent contours of the topography.

domains of E_1 and E_3, which tend to E_2. The separatrix appears to have a complicated structure and its geometry can only be approximated by a large number of time integrations of the system. As concluded by Charney and DeVore (1979) the presence of topography is a necessary condition for the existence of multiple equilibria; the unstable equilibrium E_2 is due to topographic instability. Furthermore, these authors argue that the flow patterns of the stable equilibria E_1 and E_3 resemble large scale preference states of the atmospheric circulation. Källen (1981) has drawn similar qualitative conclusions for a three component spectral model of the barotropic potential vorticity equation on a sphere.

The model is unrealistic in the sense that it always ends up in an equilibrium. For a system resembling more closely the dynamics of the atmosphere, we expect frequent transitions between the equilibria. This can be realized in two different ways. First, stochastic forcing terms can be added to the spectral equations which are thought to represent effects of the truncated models in the eigenfunction expansion, see Egger (1981) and De Swart and Grasman (1987). If the model has three equilibria, the noise forces the system to visit alternately the two attraction domains of the stable equilibria. During a transition it will remain for some time

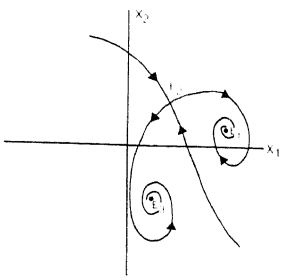

Fig. 6. Sketch of the phase flow projected onto the $x_1 - x_2$ plane. Initial conditions are chosen in a plane $x_3 =$ constant.

in a neighbourhood of the unstable equilibrium. Hence the unstable equilibrium is also of dynamical significance in the stochastic model. Another way to obtain vacillation behaviour is to choose different eigenfunctions and a different topography, such that nonlinear interactions are more efficient. Following Lorenz (1980), we may consider a closed system describing the evolution of x_2, x_4 and x_6 (defined in (3.12)). Furthermore, we choose the external forcing and topography to have a (0, 2) component only and $b = \sqrt{3}$. This system can be transformed into the Lorenz (1963a) model, which is known to have vacillating chaotic solutions for a range of parameter values. However, the assumptions are not physically significant. A nongeostrophic three component model with vacillation behaviour is discussed in Lorenz (1984).

In all these cases, characteristic residence times of the system near the equilibria are in the order of months instead of days, as expected from observations of the atmospheric circulation. Thus, we conclude that, although there is some qualitative agreement, the three component model does not give a realistic picture of the time evolution of large-scale atmospheric flow. It therefore becomes useful to include more models and study its consequences for the solutions as $t \to \infty$. This brings us to a six-component model.

4.3. SIX COMPONENTS

The six coefficient model in (4.1) between the dashed lines describes the evolution of two zonal flow profiles and two planetary wave modes. The increased number of degrees of freedom allows for a new physical mechanism, called barotropic instability. It may occur in the triad interaction between the (0, 2), (1, 1) and (1, 2) mode. Fjørtoft (1953) showed that such a triad conserves kinetic energy as well as entrophy (squared relative vorticity). Next he derived a necessary condition for a participating mode to become unstable: its wavelength must be smaller than that of the second participating mode and larger than that of the third one. Applying this theorem to the triad of the six-component model we find

$$\begin{aligned} &\text{if } b^2 < 3\text{: (0, 2) mode can become unstable,} \\ &\text{if } b^2 > 3\text{: (1, 1) mode can become unstable.} \end{aligned} \tag{4.11}$$

Thus the width-length ratio of the channel controls the barotropic wave triad.

We will now study the set of limit points of the model. First we consider the case that $x_4^* = 0$. Then, if x_4, x_5 and x_6 are zero initially, they remain zero for all times and the evolution is governed by the three component model of Section 4.2. Consequently, the equilibria of the three component model are also equilibria of the six-component model with $\hat{x}_4 = \hat{x}_5 = \hat{x}_6 = 0$; they are called single-mode equilibria. However, their stability may change due to the presence of more modes. It can be shown that the characteristic equation, which is of sixth degree in this case, factorizes into two cubic equations describing the stability with

respect to the first mode and second mode perturbations, respectively. According to the Fjørtoft theorem, equilibrium E_1 cannot become barotropically unstable, because it is characterized by a large (0, 1) component having the smallest wavenumber of the spectrum. The possible instability of E_2 and E_3 with respect to second mode perturbations can lead to additional mixed mode equilibria, for which $\hat{x}_4, \hat{x}_5, \hat{x}_6 \neq 0$, as well as periodic solutions. Charney and DeVore (1979) showed that the mixed mode equilibria are governed by

$$\begin{aligned} &d_2(\hat{x}_1)\hat{x}_4^4 + d_1(\hat{x}_1)\hat{x}_4^2 + d_0(\hat{x}_1) = 0, \\ &e_2(\hat{x}_1)\hat{x}_4^4 + e_1(\hat{x}_1)\hat{x}_4^2 + e_0(\hat{x}_1) = 0, \end{aligned} \tag{4.12}$$

where d_2, d_1, d_0, e_2, e_1 and e_0 are known functions of $\hat{x}_1$. Furthermore, for each $\hat{x}_1$ and $\hat{x}_4$ we obtain a unique $\hat{x}_2$, $\hat{x}_3$, $\hat{x}_5$ and $\hat{x}_6$. Since (4.12) is two quadratic equations for $\hat{x}_4^2$, we conclude that mixed mode equilibria always occur in pairs having the same $\hat{x}_1$, $\hat{x}_2$ and $\hat{x}_3$ component, but opposite $\hat{x}_4$, $\hat{x}_5$ and $\hat{x}_6$ components.

In the bifurcation diagram, mixed mode equilibria branch off from single mode equilibria by ordinary bifurcations, in which a real eigenvalue passes through zero. For these parameter values the (1, 2) Rossby mode is in phase with the topography. Another possibility is that the real parts of two complex conjugated eigenvalues pass through zero. At these Hopf bifurcation points periodic solutions with initial amplitude zero branch off. The latter can be interpreted as topographically modified, barotropic travelling Rossby waves. Charney and DeVore (1979) have shown that such solutions indeed exist. To study the dependence of these solutions on parameters is complicated and can only be done numerically. Their stability properties can change too, leading to possible doubly periodic, quasi-periodic- and chaotic solutions. Studies on the attractor properties of the model have been carried out by Yoden (1985) and de Swart (1987a). We now discuss results for the parameter values defined in the previous subsection.

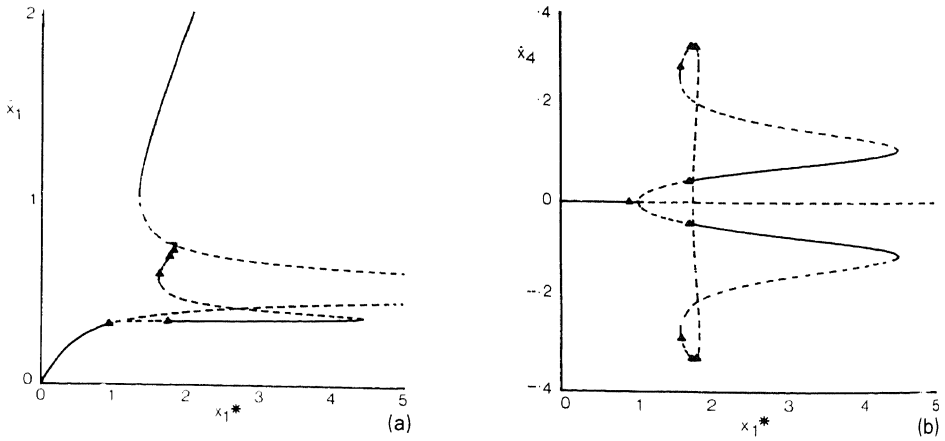

Fig. 7. As figure 4b, but solution components $\hat{x}_1$ and $\hat{x}_4$ of the six component model as a function of x_1^* for $x_4^* = 0$, $\gamma = 1$. The triangles denote Hopf bifurcation points.

In Figure 7 the $\hat{x}_1$ and $\hat{x}_4$ component of the stationary points are shown as a function of x_1^* for $x_4^* = 0$ and $\gamma = 1$. Comparison with Figure 4b shows that mixed mode equilibria branch off from the single mode equilibria by pitchfork bifurcations. Depending on the value of x_1^* there can be one up to eleven equilibria. All of them are connected by means of limit points in the bifurcation diagram, i.e., there are no isolated equilibria. As can be seen many of them are unstable with respect to small perturbations. For $0.932 \leq x_1^* \leq 1.336$ no stable stationary points are obtained. Numerical integrations for these parameter values show that trajectories starting from arbitrary initial conditions tend to a globally attracting limit cycle.

The bifurcation diagram contains nine Hopf bifurcations, where we expect periodic solutions to branch off. In Figure 8 the period of the orbits emanating from E_3 at $x_1^* = 0.932$ is shown as a function of x_1^*. At the Hopf bifurcation point, the period is $2\pi/\sigma_i$, where σ_i is the imaginary part of the two eigenvalues with real part zero, while the amplitude is zero. Time series of the x_1 and x_4 component, as well as projections of the orbits onto the $x_1 - x_4$ plane, are shown in Figure 9 for various parameter values.

It appears that the stable periodic solutions bifurcate on the side of the unstable equilibrium E_3, hence it is a super-critical Hopf bifurcation, see Guckenheimer and Holmes (1983). With increasing x_1^* the amplitude of the periodic orbits increases, while the period decreases a little. The behaviour of the solution becomes more complicated because of the higher harmonics of the fundamental frequency (Figure 9a, b). Note that the orbits are symmetric with respect to $x_4 = 0$, $x_5 = 0$, $x_6 = 0$. However, at $x_1^* = 1.561$ the symmetry is broken by a pitchfork bifurcation. The symmetric, periodic orbit becomes unstable while two nonsymmetric stable periodic orbits branch off. One of them is shown in

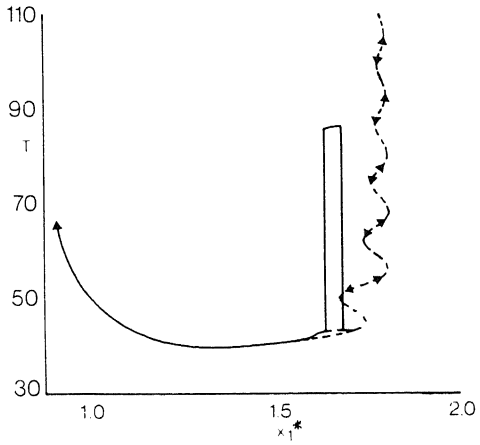

Fig. 8. Period T of the periodic orbits emanating from the E_3 branch of stationary points as a function of x_1^*, $x_4^* = 0$, $\gamma = 1$. Solid curves denote that the orbit is stable, while dashed curves refer to unstable orbits. The symbols —< and >— denote sequences of period doublings and period halvings in a very small region of x_1^* values, respectively.

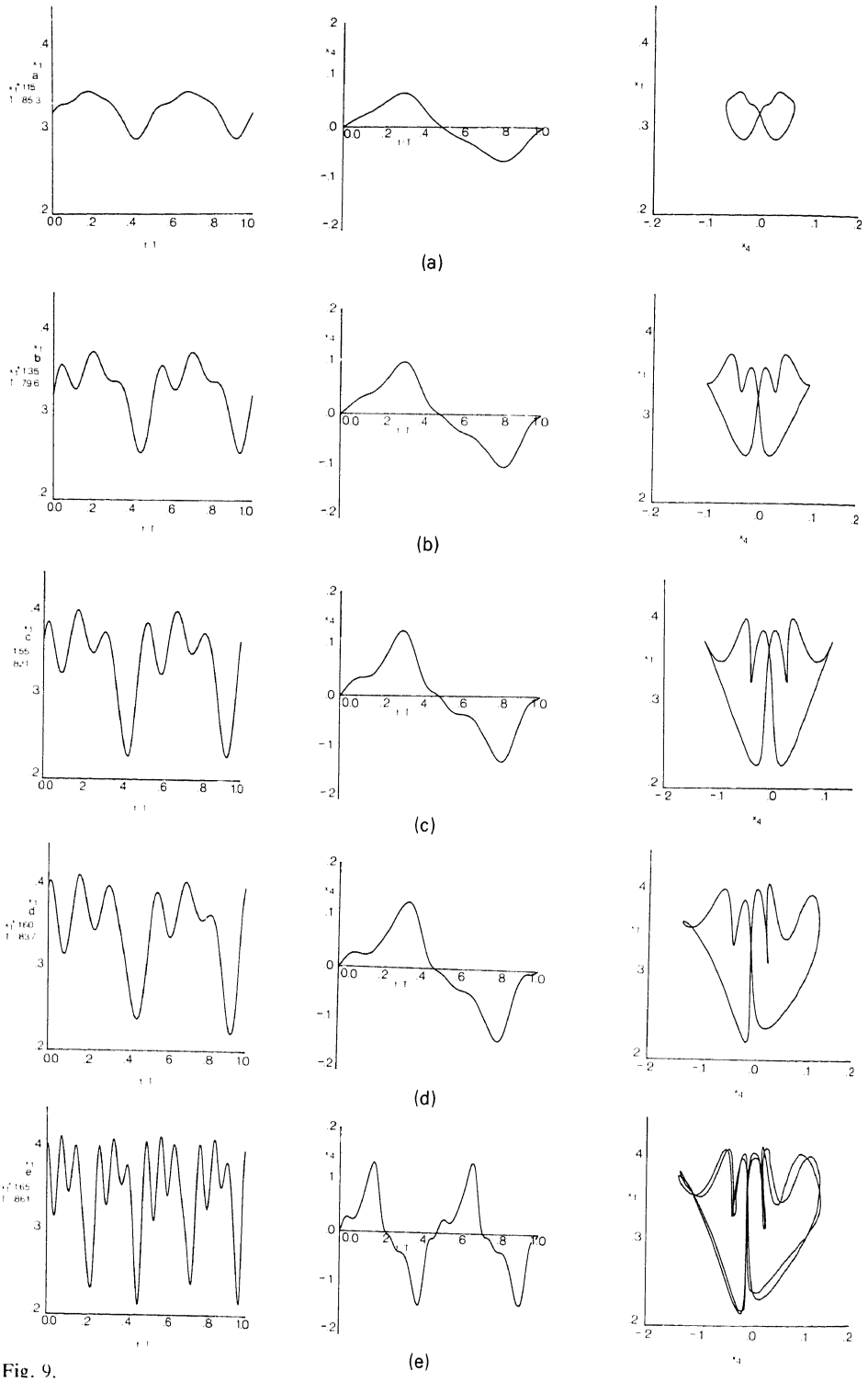

Fig. 9.

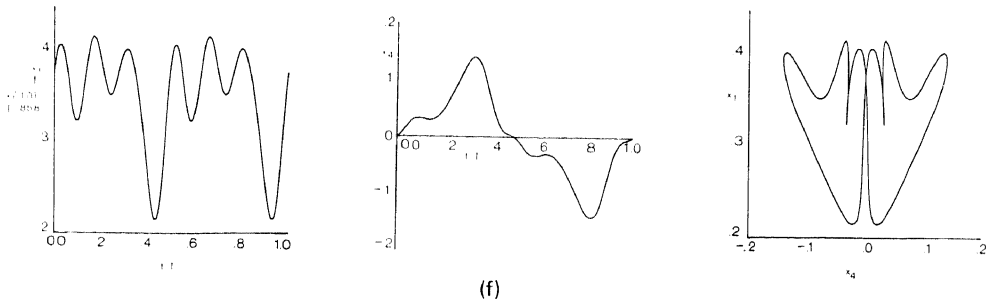

(f)

Fig. 9. Visualization of some stable periodic solutions discussed in Section 4.3, see Figure 8. Shown are $x_1(t/T)$, $x_4(t/T)$ and the projection of the orbits onto the $x_1 - x_4$ plane. Here t is time and T the period.

Figure 9c, the other is obtained by reflection in $x_4 = 0$. Each of the nonsymmetric orbits becomes unstable at $x_1^* = 1.638$ due to a period doubling bifurcation. At these points stable periodic orbits with twice the period branch off. An example of such a solution is shown in Figure 9d. Further period doubling bifurcations do not take place. On the contrary, we have a period halving bifurcation at $x_1^* = 1.684$ and a pitchfork bifurcation at $x_1^* = 1.716$.

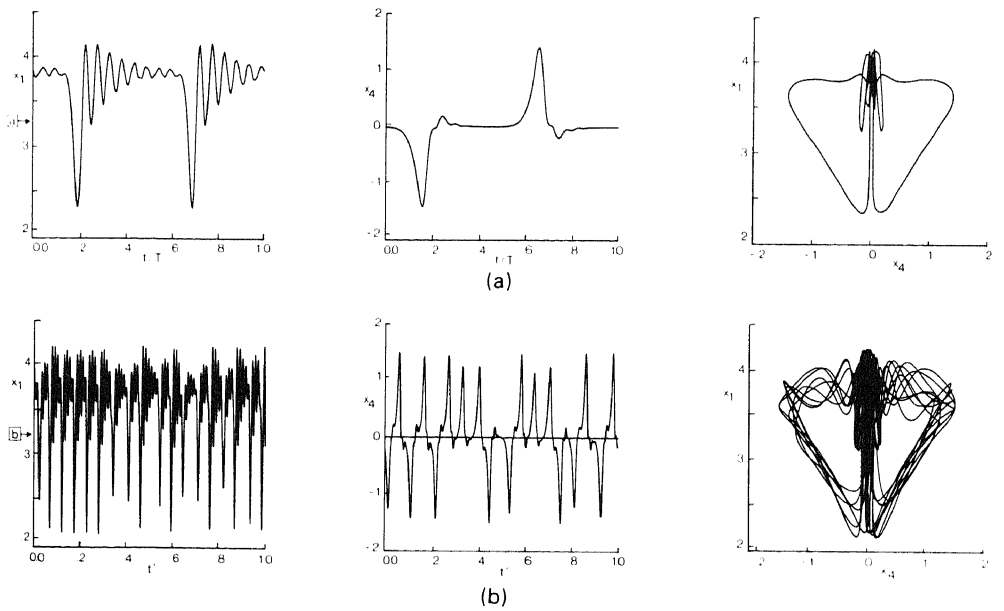

(a)

(b)

Fig. 10. (a) Numerical approximation of the homoclinic orbit at $x_1^* = x_{1,c}^*$ as a periodic orbit with a large period, here $T \approx 120$. Shown are the x_1 and x_4 component as a function of t/T, as well as the projection of the orbit onto the $x_1 - x_4$ plane. (b) Chaotic time series for $x_1^* = 1.75$ started in the unstable equilibrium E_3. Shown are the x_1 and x_4 component as a function of $t' = t/500 - 1$ as well as a projection of the trajectory onto the $x_1 - x_4$ plane. Transient effects have already died out before entering the time interval shown.

A further increase of x_1^* complicates the structure of the remaining branch of symmetric periodic orbits. In the region $1.67 \leq x_1^* \leq 1.81$ it shows a series of wiggles with an increasing period, the latter tending to infinity as $x_1^* \to x_{1,c}^* = 1.79$. The wiggles are saddle node bifurcations, in which a stable- and unstable periodic orbit coalesce. The tendency of the period to become infinitely large is associated with the approach to a homoclinic orbit existing for $x_1^* = x_{1,c}^*$. A numerical approximation of this orbit is shown in Figure 10a. It connects the unstable saddle point E_3 with itself. This type of bifurcation has been analyzed by Silnikov (1965) and more recently by Glendinning and Sparrow (1984). They showed that in the neighbourhood of the homoclinic orbit a countable infinity of unstable periodic orbits exist. Furthermore, an uncountable infinity of aperiodic chaotic orbits occur, which are generated and absorbed by an infinite cascade of period doubling and periodic halving bifurcations, respectively. They take place near each winding of the $T(x_1^*)$ curve in Figure 8. An example of a chaotic time series, for $x_1^* = 1.75$, is shown in Figure 10b. Note that the trajectories move in a small tube, which closely resembles the homoclinic orbit. The importance of this type of bifurcation for spectral models of the atmospheric circulation has already been proposed by De Swart and Grasman (1984).

Yoden (1985) also studied the bifurcation properties for different topography amplitudes. In De Swart (1987a) other channel geometries are considered and the effect of nonzero x_4^* is studied. From their results it appears that for all parameter values the set of limit points at least contains a stable stationary point or a stable periodic orbit. It appears that the strange attractors have only a limited attraction domain in phase space. Hence, it is concluded that a six component barotropic spectral model has not sufficient degrees of freedom to allow for a global strange attractor. In other words, although the model shows a rich internal dynamics, it cannot describe an index cycle, i.e., an aperiodic vacillation between zonal- and meridional-preference states. This can be met by either adding stochastic perturbations to the equations or introducing more degrees of freedom. We will review the second possibility.

4.4. HIGHER-ORDER MODELS

If more modes are included in the spectral expansions, in order to obtain a system with dynamics qualitatively similar to those of the atmosphere, we obtain more complex spectral equations and their mathematical analysis becomes rather difficult. For example, stationary points are governed by a set of M nonlinear algebraic equations and already for moderate M it is generally impossible to solve this system analytically. In these cases numerical methods should be applied. This can be done by using a continuation technique. Knowing a stationary point $\hat{\mathbf{x}}(\mu)$ of the vector field $\mathbf{f}_\mu(\mathbf{x})$ for the parameter value μ, a nearby stationary point $\hat{\mathbf{x}} + \Delta\mathbf{x}$ for $\mu + \Delta\mu$ is obtained from

$$\Delta \mathbf{x} \cdot \nabla \mathbf{f}_\mu(\hat{x}) + \Delta\mu \frac{\partial}{\partial \mu} \mathbf{f}_\mu(\hat{\mathbf{x}}) = 0. \tag{4.13}$$

This system can be solved numerically with the pseudo-arclength method developed by Keller (1977). In this way a complete exploration can be made of a one-parameter branch of stationary solutions. Periodic solutions emanating from Hopf bifurcation points can be studied in a similar way. Recently the package AUTO of Doedel (1986) has become available. It contains routines to locate branches of stationary and periodic solutions in parameter space using the pseudo-arclength continuation method. Furthermore, the local stability of the solutions is determined and an accurate location of turning points and bifurcation points is given. Periodic solutions are found by solving an associated boundary-value problem such that no *a priori* choice of a Poincaré return map is required. However, the technique requires a large computer storage and is therefore incapable to handle systems with $M > 6$.

Legras and Ghil (1985) were the first to investigate the analytical properties of a higher-order barotropic spectral model. Although they took a spherical domain instead of a beta plane, we will discuss their results briefly. In their paper the pseudo-arclength method is used to locate stationary points of a 25-component model. For various values of the forcing, dissipation and topography parameters, they obtained multiple equilibria, including some which resemble those of Charney and DeVore (1979). The latter, which are due to topographic instability, occur for unrealistically large values of the forcing ($\geq 100\,\mathrm{ms}^{-1}$). For smaller forcing values multiple equilibria of the mixed-mode type appear, which can be classified in high index, low index and transitional states.

Next, Legras and Ghil (1985) investigated the existence of periodic and aperiodic motions by integrating their system for a large number of different parameter values and initial conditions. They concluded that the model may exhibit properties of an index cycle. The corresponding strange attractor in phase space is folded in a complicated way around some of the unstable stationary points, which resemble quasi-stationary preference states of the model. Obviously unstable equilibria may be significant for the atmospheric dynamics.

The regime predictability was studied by computing residence times of the system in regions of phase space enclosing the preference states. The dynamics of the index cycle appears to depend strongly on the forcing: for small forcing the low index state is most preferent, for a slightly increased forcing the high-index state is visited more often. This sudden change in the structure of the strange attractor is called a crisis, see Grebogi *et al.* (1986). Using realistic forcing values characteristic residence times of the system in the preferent regimes are of the order of weeks. This is large compared to the typical life of a quasi-stationary preference state of the atmospheric circulation, being of the order of days. Legras and Ghil (1985) propose that this is a consequence of the severe truncation and, therefore, even more modes should be included in the spectral expansions to remove this problem.

For a beta plane channel geometry, De Swart (1987b) has derived a minimum order spectral model, which allows for the existence of vacillatory solutions and which has two clearly distinguishable length scales: a planetary and synoptic scale. The result is the ten component model (4.1). The case $C = 0.1$, $\beta = 2$, $\gamma = 1$, $b = 1.6$, $x_1^* = 2.5$ and variable x_4^* is considered in detail. The physical situation is nearly identical to that in the Sections 4.2 and 4.3. However, the channel-width is reduced from 5000 to 4000 km and, furthermore, the external forcing may also act on the (0, 2) zonal flow component. This is done in order to allow for barotropic instability of the high-index equilibrium E_1, being a necessary condition to obtain vacillation behaviour, see (4.11).

It appears that for $|x_4^*| > 4$ the model possesses a global strange attractor, to which trajectories starting from arbitrary initial conditions converge. A typical nontransient time series of the x_1 component is shown in Figure 11a for the value $x_4^* = -5$. Here x_1 measures the zonal eastward transport between the two meridional channel-walls and can thus be interpreted as a zonal index. Again it is found that solutions aperiodically visit three different preferent regimes, which are of high index, low index and transitional type, respectively. In phase space these preferent regions are not characterized by unstable stationary points, such as in the model of Legras and Ghil (1985), but by unstable periodic orbits. The residence times of the system in the different regimes are again of the order of months. Therefore, De Swart (1987b) concludes that the 10 coefficient model reflects most qualitative properties of the atmospheric circulation, but for a more realistic picture higher-order models should be used.

The concept of the strange attractor also provides a way to study the predictability problem, which was already mentioned in the introduction. Chaotic

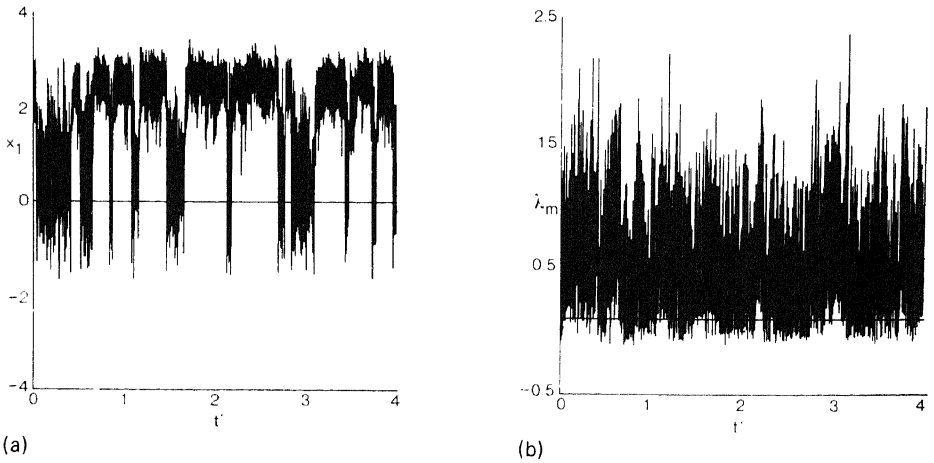

Fig. 11. (a) Nontransient time series of the x_1 component of the ten-component model (4.1), which is proportional to the zonal index. The period shown is approximately eight years, for parameter values see text. (b) Time series of the maximum real part λ_m of the eigenvalues of the phase flow, linearized at each point of the orbit shown in Figure 11a. Here $t' = t/500 - 1$.

motion is characterized by sensitive dependence on the initial conditions, i.e., nearby orbits exponentially diverge during the evolution of the system. Since in practical situations initial conditions are not known with infinite precision, this property might explain the finite predictability of the atmospheric circulation. A quantitative measure of predictability is provided by the Lyapunov exponents of the system. They measure the average exponential growth of the principal axes of an infinitesimal small error sphere along the orbit. Wolf *et al.* (1985) have developed methods to compute them numerically. A chaotic time series has one or more positive Lyapunov exponents and the reciprocal of the largest positive number defines a mean time-scale on which the system is predictable. For the time series of Figure 11a this time scale is a few days, which seems a realistic value for large-scale atmospheric flow.

However, in practice, predictability will vary in time since it depends on the particular state of the flow. Studies with numerical weather prediction models have shown that the validity of forecasts varies between a day and two weeks. It is proposed by Legras and Ghil (1985) and De Swart (1987b) that a lower bound of the point predictability is given by the reciprocal of the largest real part λ_m of the eigenvalues of the phase flow, linearized at each point of the orbit. The eigenvector corresponding to λ_m defines the associated most unstable eigenmode, its structure showing the geographical distribution of the error-growth. In Figure 11b λ_m of the ten component model (4.1) is shown as a function of time for the same conditions used in Figure 11a. As can be seen the predictability largely varies during the period. In particular, there are short time intervals where λ_m is negative. During these periods small errors will converge to the principal orbit. Relating this to weather predictions, we conclude that as long as during a specific forecast λ_m is negative it is preferrable to continue this forecast run instead of starting a new run. This is because deviations between the old forecast and true solution have been decreased during the integration, while re-initializing would certainly cause larger errors. For more details we refer to De Swart (1987b).

5. Two-Level Baroclinic Models

5.1. INTRODUCTORY REMARKS

In this section we will study some low-order spectral models of a two-level version of the quasi-geostrophic potential vorticity equation in a beta plane channel, see Appendix C. For nonzero $\sigma_0 = (F')^{-1}$, y_1^* or y_4^* vertical gradients are created, which allow for a new physical mechanism, called baroclinic instability. This is an important mechanism, which is responsible for the generation of transient eddies from the planetary scale flow (Pedlosky, 1979).

We will consider flows which are driven in the (0, 1) baroclinic mode only ($x_1^* = x_4^* = y_4^* = 0$, y_1^* nonzero), as is done in all papers so far. Charney and

Straus (1980) have shown that in this case

$$y_1^* = \frac{Rl^2}{4\sqrt{2}\sigma f_0}\Delta\theta^*. \tag{5.1}$$

Here R is the gas constant for dry air and $\Delta\theta^*$ is the potential temperature gradient between the northern and southern wall of the channel. Despite its great complexity, we can easily derive some properties of this 20-component model. First, the equations are invariant under the transformation

$$\begin{pmatrix} x_1, x_2, x_3, x_4, x_5, x_6, x_7, x_8, x_9, x_{10} \\ y_1, y_2, y_3, y_4, y_5, y_6, y_7, y_8, y_9, y_{10} \end{pmatrix} \rightarrow$$
$$\begin{pmatrix} x_1, x_2, x_3, -x_4, -x_5, -x_6, -x_7, -x_8, x_9, x_{10} \\ y_1, y_2, y_3, -y_4, -y_5, -y_6, -y_7, -y_8, y_9, y_{10} \end{pmatrix}. \tag{5.2}$$

Secondly, nontrivial stationary points can be obtained by putting all amplitudes equal to zero with exception of the (0, 1) modes. We then find

$$\hat{x}_1 = \hat{y}_1 = \frac{a}{a + 2\sigma_0 C'} y_1^*. \tag{5.3}$$

The corresponding streamfunctions at the levels $z = z_1$, $z = z_2$ and the vertical velocity field read

$$\begin{aligned} \Psi(z_1) &= \frac{2\sqrt{2}a}{a + 2\sigma_0 C'} y_1^* \cos(y), \\ \Psi(z_2) &= 0, \\ w_1(h_2) &= \frac{2\sqrt{2}a}{a + 2\sigma_0 C'} C'F' y_1^* \cos(y), \end{aligned} \tag{5.4}$$

where use has been made of (3.3) and (3.7). A sketch of the circulation pattern of this so-called Hadley state is shown in Figure 12. There is no horizontal flow at the lower level and the vertical velocity field is caused by heating and the

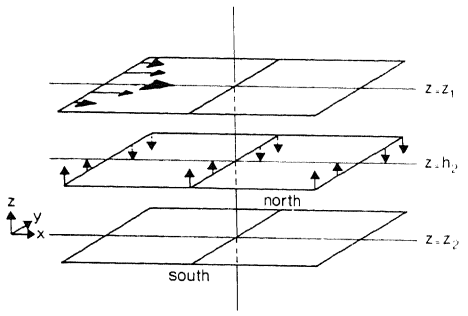

Fig. 12. Three-dimensional circulation pattern of the Hadley equilibrium state defined by (5.4).

presence of internal friction. Its stability depends on the parameters as well as the number of resolved modes. At bifurcation points new stationary points or periodic solutions will branch off, which may result in a very complicated dynamics.

Before studying the full 20-component model we will consider two subsystems. By including only the (0, 1) and (1, 1) modes we arrive at a six-component model for the amplitudes x_1, x_2, x_3, y_1, y_2 and y_3. Similarly, by including only the (0, 1), (0, 2), (1, 1) and (1, 2) modes a 12-component model is obtained. They will be discussed in the next subsections.

5.2. SIX COMPONENTS

Consider the equations for x_1, x_2, x_3, y_1, y_2 and y_3, (C1)–(C3), (C11)–(C13) in Appendix C between the dotted lines, with $x_1^* = x_4^* = y_4^* = 0$. They describe the interaction of a zonal flow and a planetary wave mode in a two-level version of the quasi-geostrophic potential vorticity equation. It is the simplest baroclinic extension of the three-component barotropic model discussed in Section 4.2. Note that if in the twenty component model the amplitudes of the (0, 2), (1, 2), (2, 1) and (2, 2) modes are taken zero initially they remain zero for all times. Consequently, solutions of the six component model are also solutions of the full model under the conditions mentioned above, although the stability properties can be quite different.

Concerning the stationary points, we have already obtained the Hadley state in the previous subsection. Small perturbations on this state evaluate proportional to $\exp(\lambda t)$, where the eigenvalues λ are the zeros of a polynomial equation of sixth degree in λ. For $y_1^* \to 0$ all roots have negative real parts, consequently the Hadley state is stable. If the forcing is increased instabilities can be generated in two different ways. First a Hopf bifurcation can occur, where the real parts of two complex conjugated roots change sign. Then periodic solutions are generated which can be interpreted as travelling baroclinic waves. A necessary condition for this baroclinic instability of the Hadley state is

$$\sigma_0 b^2 < 1, \tag{5.5}$$

as is found from standard perturbation theory. Secondly, the Hadley state can become unstable by an ordinary bifurcation, where a real eigenvalue changes sign. This mechanism can only occur for nonzero γ, therefore it is called topographic instability. A resonance condition is derived in a similar way as for the three-component model of Section 4.2. In the unforced, nondissipative case it reads

$$2\alpha_{11}\hat{x}_1 - \beta_{11} = 0. \tag{5.6}$$

We now have a growing wave disturbance on the upper level which is stationary with respect to the topography. For $\hat{x}_1 < (>) \beta_{11}/2\alpha_{11}$ the Hadley state is topo-

graphically stable (unstable). A procedure for computing all stationary points of the model is presented in Charney and Straus (1980). They conclude that the presence of topography is necessary in order to obtain multiple equilibria.

As an illustrative example we present stationary points as a function of the forcing y_1^* for the parameter values $b = 1.06$, $\gamma = 1$, $C = 0.057$, $\beta = 2.5$, $C' = 0.114$, $a = 0.114$ and $\sigma_0 = 0.2$. This corresponds to a channel with length 9434 km and width 5000 km. The topography amplitude is one tenth of the scale height, the Ekman dissipation time scale is 20 days and time scales for internal friction and Newtonian cooling are taken to be 10 days. In Figure 13 $(\hat{x}_1 - \hat{y}_1)$, and the $\hat{x}_2$ component of the stationary points are shown as a function of y_1^*. Here $(\hat{x}_1 - \hat{y}_1)$ measures the zonal flow intensity at the lower level and $\hat{x}_2$ the barotropic wave amplitude being in phase with the topography.

For small forcing values we have the Hadley state as the only equilibrium and a linear stability analysis shows that it is stable. At $y_1^* = 1.32$ two new branches of stationary points appear. They are called branch 1 and branch 2 equilibria (Charney and Straus, 1980) or a 45° trough and 90° ridge state (Reinhold and Pierrehumbert, 1982), where the degrees denote the phase difference of the trough (or ridge) with respect to the topographic maximum. In a small region of y_1^*, between 1.32 and 1.33, the branch 2 equilibrium is unstable. At $y_1^* = 1.33$ it becomes stable, while the Hadley state becomes topographically unstable. Baroclinic instabilities on the 90° ridge, 45° trough and the Hadley state occur at $y_1^* = 1.37$, $y_1^* = 1.50$ and $y_1^* = 1.64$, respectively. The 45° trough becomes stable again at $y_1^* = 1.76$. For forcing values between 1.78 and 2.03, five stationary points exist. The new ones are called branch 3 (30° ridge) and branch 4 (near Hadley) equilibria, which appear only if the Hadley state is baroclinically unstable. They are both unstable, except for y_1^* between 1.78 and 1.79 where the near Hadley state is stable. For $y_1^* > 2.03$ three equilibria remain, the 45° trough

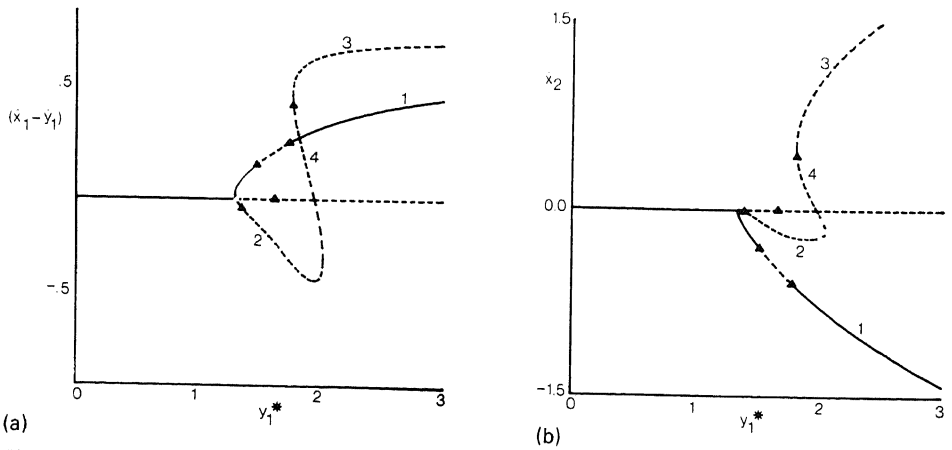

Fig. 13. Stationary solutions of the six-component baroclinic model for the wave number 3 situation discussed in the text. Shown are $(\hat{x}_1 - \hat{y}_1)$ and $\hat{x}_2$ as a function of the thermal forcing y_1^*. Branch numbers are also indicated. The triangles denote Hopf bifurcation points.

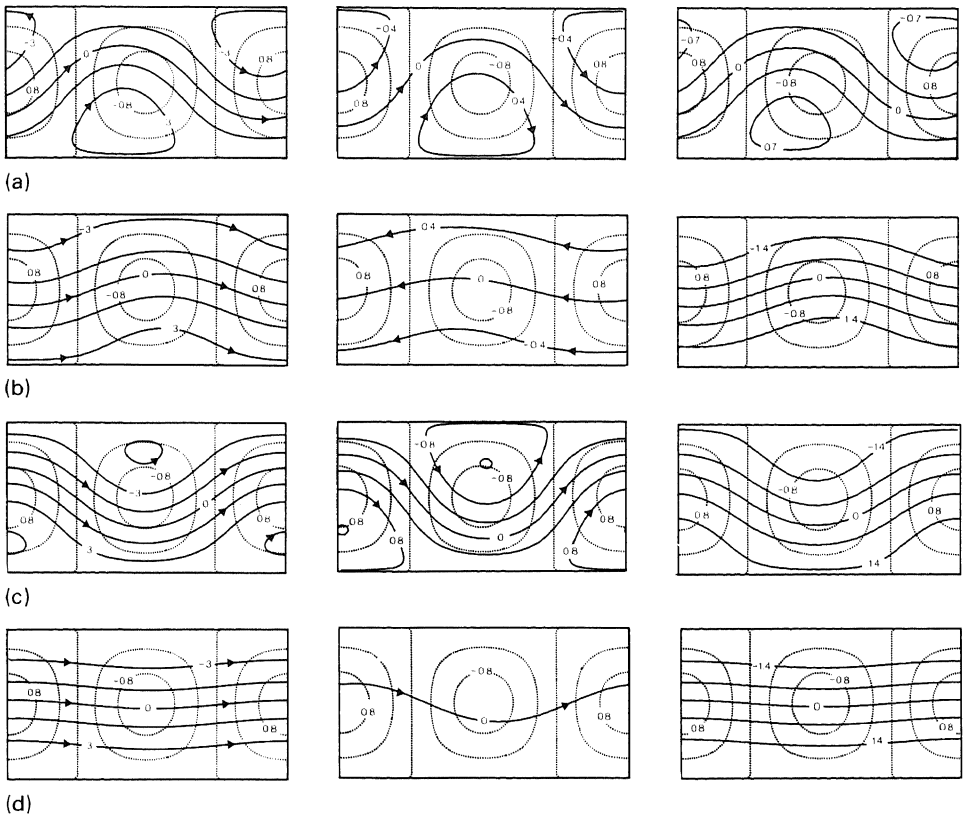

Fig. 14. Contour plots (solid curves) of the nondimensional streamfunction patterns at the upper level (left) and lower level (middle), as well as the nondimensional potential temperature distribution (right) of the branch 2 (a), branch 3 (b), branch 4 (c) and branch 5 (d) equilibria discussed in the text. Arrows denote the direction of the flow $\Delta\psi = 1$ corresponds to a zonal transport of $2.7 \times 10^7\ m^2 s^{-1}$, $\Delta\theta = 1$ corresponds to a potential temperature difference of $0.1.\theta_s$ where θ_s is defined by (2.5). The dashed curves represent contours of topography (km).

being stable. Obviously the model contains one, three or five stationary points. In Figure 14 the streamfunction patterns at the upper and lower level, as well as the potential temperature distribution at the intermediate level are shown for the four wavy equilibria existing at $y_1^* = 1.85$.

Application of (5.1) gives that this forcing corresponds to a temperature difference of 95 K between the northern and southern wall of the channel. This unrealistically large value, necessary to obtain multiple equilibria, is probably due to the severe truncation. The 45° trough and 90° ridge equilibria resemble low-index states with large wave amplitudes and weak zonal flows. On the other hand, the Hadley, near Hadley, and 30° ridge equilibria can be characterized as high-index states with large upper-layer zonal flows (of order $60\ ms^{-1}$) and relatively weak wave-fields. All equilibria have a typical baroclinic structure in the sense that they display westward phase shifts with height. Such structures are also observed in the atmosphere.

To see whether the calculated equilibria are important for the system dynamics, Charney and Straus (1980) carried out a large number of numerical integrations for various forcing values and different initial conditions. From their results it follows that for y_1^* smaller than 1.32 all trajectories converge to the stable Hadley state. For larger forcing values solutions either converge to a steady state or to a limit cycle, but not to a strange attractor. Even if a strange attractor exists, it will only be part of the full set of limit points, because for all forcing values there is at least one stable steady state or stable limit cycle. Obviously, for the parameter regime under consideration the model cannot describe an index cycle. A clearly different behaviour is found by halving the length of the channel, resulting in $b = 2.12$ (zonal wave-number 6). Figure 15 shows $(\hat{x}_1 - \hat{y}_1)$ and the $\hat{x}_2$ component of the stationary points for this new model as a function of y_1^*.

In this case one or three stationary points are obtained and for $y_1^* > 0.70$ none of them is stable. For large forcing values, Charney and Straus (1980) found aperiodic solutions, but they did not analyze them in great detail. They argue that the wavenumber 6 situation is not representative for the planetary scale circulation. A more realistic model is provided by the wavenumber 3 case studied previously, but then no vacillation behavior is found. This suggests that higher resolution models are needed and they will be the subject of the rest of this section.

5.3. TWELVE COMPONENTS

A second baroclinic subsystem of the spectral model ((C1)–(C6), (C11)–(C16) in Appendix C between the dashed lines) consists of equations for x_i and y_i, with $i = 1, 2, \ldots, 6$. It can be seen as an extension of the spectral model discussed in Section 4.3 to two levels. It allows for topographic, barotropic and baroclinic

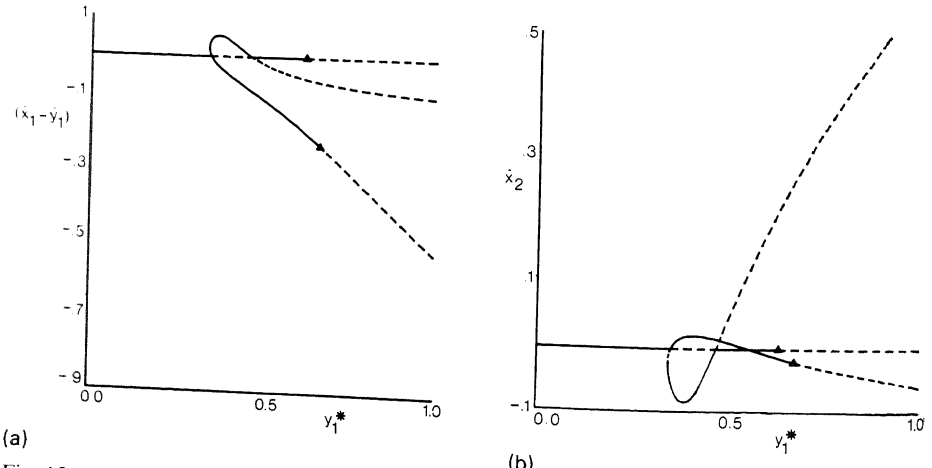

Fig. 15. As Figure 13, but for the wavenumber 6 situation.

instabilities, but no wave triad interactions are present. Note that solutions of this subsystem are not generally solutions of the full model of Appendix C.

In the bifurcation diagram stationary points of the six component subsystem will also be stationary points of the 12-component model, but their stability can change due to the presence of more degrees of freedom of the perturbations. At the possible bifurcation points mixed mode equilibria or periodic solutions will branch off. In Figure 16 we show $(\hat{x}_1 - \hat{y}_1)$ and the $\hat{x}_2$ component of the stationary points as a function of the forcing y_1^* for the wavenumber 3 situation discussed in Section 5.2.

Comparison with Figure 13 shows that no mixed mode equilibria occur. A Hopf bifurcation point at $y_1^* = 0.93$ turns all stationary points unstable for $y_1^* > 0.93$. Consequently, the attractor properties will be considerably different from the six-component model, which is confirmed by the numerical experiments of Charney and Straus (1980) and Yoden (1983a). Depending on the value of the forcing and initial conditions they obtained solutions converging to a stationary point or a limit cycle, but also aperiodic solutions. The question whether this model has a global strange attractor, with associated vacillation behaviour, remains to be studied.

5.4. TWENTY COMPONENTS

We will now study the full 20-component model of Appendix C with forcing in the baroclinic (0, 1) mode only ($x_1^* = x_4^* = y_4^* = 0$). It describes the interaction of two zonal flow modes and four wave modes in a two-level version of the quasi-geostrophic potential vorticity equation in a beta plane channel. The model was introduced by Reinhold and Pierrehumbert (1982). They studied the feedback mechanism between the planetary wave regime, represented by the (1, 1) mode, and the synoptic regime represented by all other wave modes. This

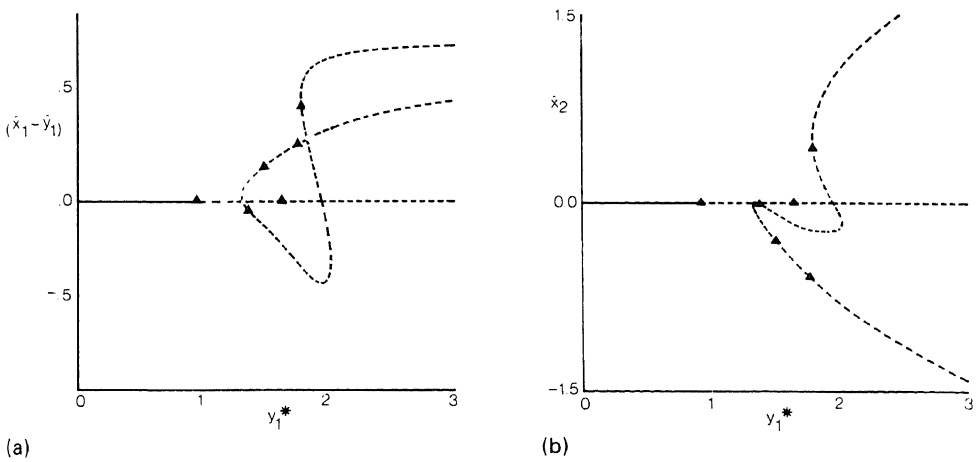

Fig. 16. As Figure 13, but for the twelve-component baroclinic model.

feedback is provided by wave triads, not being present in the baroclinic models studied so far. They generate direct interactions between the (1, 1), (1, 2) and (2, 1) modes, see also Yoden (1983b).

A systematic bifurcation analysis of the model is complicated and up to now no attempt has been made to carry it out. We only know that the Hadley state is always an equilibrium and that solutions of the six-component model of Section 5.2 are also solutions of the full model. Here we will take the parameter values $b = 1.3$, $C = 0.5$, $\gamma = 4$, $\beta = 2$, $C' = 0.1$, $a = 0.45$, $\sigma = 0.1$ and $y_1^* = 1.8$, being similar to the demonstration case of Reinhold and Pierrehumbert (1982). Here the flow is considered in a channel of length 6155 km and width 4000 km. The time scales for barotropic dissipation and Newtonian cooling are two days and for internal friction 10 days. Furthermore, the topography amplitude is chosen 4 km and the north-south wall temperature difference is set at 60 K. There are five single mode equilibria in this case, which are the Hadley state, the near Hadley state, the 90° ridge state, the 45° trough state and the 30° ridge state. Their flow configurations are qualitatively similar as those presented in Figure 14 for the Charney and Straus (1980) model. All of them appear to be unstable with respect to small perturbations.

Next the attractor properties of the model are studied by constructing and analyzing a long time series. In Figure 17 a projection of the phase space trajectory is presented on the $x_2 - x_3$-plane, constructed by plotting daily values of the x_2 and x_3 components during a dimensional time integration period of 15 years. It shows the climatology of the (1, 1) barotropic mode.

As can be seen only a limited range of phases are visited by the system. Further analysis shows that this mode aperiodically vacillates between two preferent regions, i.e., a trough and ridge regime represented in Figure 17 by the upper left

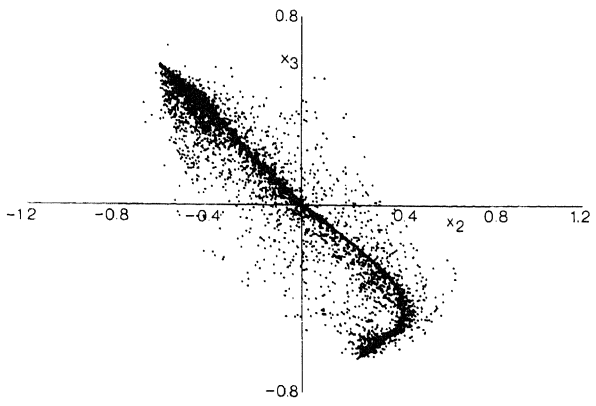

Fig. 17. Climatology of the (1, 1) barotropic wave mode of the 20-component baroclinic model for the demonstration case discussed in the text. Shown are daily values of the x_2 and x_3 component for an integration period of 15 years.

and lower right quadrant, respectively. During a transition, generated internally, the system remains for some time in a third region characterized by a small amplitude of the (1, 1) mode. The time scale of the transitions (a few days) is much smaller than the characteristic persistence times of the trough and ridge regimes. The duration of a single regime event is highly arbitrary and has no dynamically preferred time scale.

The (1, 1) mode evolution has the typical characteristics of a regime cycle. However this behaviour is not found for the small-scale wave modes. Their amplitudes vary rapidly in time without having regional phase space preferences. For this reason Reinhold and Pierrehumbert (1982) distinguish between quasi-stationary planetary waves, represented by the (1, 1) modes, and transient synoptic eddies including all other wave modes. The quasi-stationary preference states of the planetary waves are called weather regimes. Qualitatively similar results are obtained for many other parameter values.

Most of the time trajectories do not come near the single mode equilibria of the model. Nevertheless, there seems to be some relation between 45° trough solution and the trough regime and between the 30° ridge solution and the ridge regime. It appears that the phase of the (1, 1) mode in the quasi-steady states is similar to those of the stationary solutions mentioned, although the amplitudes of the latter are much larger. From a more close inspection of the time evolution of the (1, 1) mode it follows that its behaviour is smooth and slow in the trough regime, while it shows oscillatory behaviour in the ridge- and transitional regime. This suggests that in phase space the trough regime is close to an unstable (mixed mode) stationary point, while the ridge and transitional regimes are close to nonstable periodic orbits of the model. These hypotheses seem to be confirmed by numerical experiments, where for each regime procedures for finding stationary and periodic solutions are carried out. The periodic orbit corresponding to the transitional regime has probably branched off from the 90° ridge solution.

Reinhold and Pierrehumbert (1982) studied the dynamic feedback between the planetary waves and the transient eddies by calculating the various vorticity budgets for the spectral model. It appears that the forcing of planetary waves by transient eddies has a characteristic time-mean structure in both the trough and ridge regime. However, the intensity of eddy forcing, as well as the effect of topography, is much smaller than that of other physical processes such as the time-mean relative vorticity advection by the time-mean flow. This suggests that topographic instability is only a triggering mechanism in order to generate multiple weather regimes, while wave-wave interactions are responsible for the transitions between the regimes.

Another interesting property is that the patterns of the transient eddy forcing, averaged over the persistence period of a weather regime, has a similar spatial structure as the baroclinically most unstable eigenmode associated with the quasi-stationary state, but with a phase difference of 180°. This fact suggests that the periods of quasi-stationary behaviour in the large scales are integrally

associated with an organized behaviour of the synoptic scales. The net forcing by the transients seems to stabilize the planetary waves: if the phase or amplitude of a planetary wave is perturbed, the result will be a change in the net transient forcing which compensates for the perturbation and forces the planetary wave back in its original state. This is confirmed by an experiment in which the mode (0, 1) and (1, 1) equations are integrated with additional terms being a statistical parametrization of the transient eddy forcing. The latter are found by calculation of the vorticity budgets associated with the baroclinically most unstable eigenmode of the full system at each time step. The reduced model appears to have two stable states which resemble the quasi-steady states obtained with the full model. The fact that the states are stable is a consequence of the removal of the oscillatory behavior of the transient eddy forcing. This confirms the idea that the instantaneous effect of the forcing is responsible for the transitions between the various weather regimes.

6. Conclusions

In this paper low-order spectral models of the quasi-geostrophic potential vorticity equation in a beta plane channel have been reviewed and new results are added. Particular attention has been paid to the studies of Charney and DeVore (1979), Charney and Straus (1980), Reinhold and Pierrehumbert (1982) and Legras and Ghil (1985). We will now discuss in what sense these models reflect properties of the large-scale atmospheric circulation.

There are two motivations to consider a barotropic version of the potential vorticity equation, as was done in Section 4. First, it gives the simplest description of quasi-geostrophic dynamics. Secondly, it appears that the long-term variability of the atmosphere has a pronounced barotropic structure (Blackmon *et al.*, 1979). This also applies to persistent anomalies of the atmospheric circulation (Dole and Gordon, 1983). The reason for this barotropic adjustment is not yet well understood.

Spectral models of the barotropic potential vorticity equation possess, in the absence of zonal asymmetries, only one equilibrium which is of the high-index type. If topographic forcing is introduced, waves are generated and multiple equilibria can be found for a range of parameter values. The flow patterns of the equilibria resemble large-scale preference states of the atmosphere. This behaviour is already present in the low-order models of Sections 4.2 and 4.3. Further details about the topographic forcing mechanism can be found in Pedlosky (1981).

To test the validity of their spectral model results, Charney and DeVore (1979) compared them with those obtained with a grid-point model, the latter having many more degrees of freedom. In many situations fairly good agreements were found. On the other hand, there are also objections against the theory. In Section

4 a channel length of 5000 km was chosen, which is a rather *ad hoc* value. Actually, the channel should encircle the earth, extending the zonal dimension to about 28 300 km at 45° latitude. In that case unrealistically large forcing values ($>100\,\mathrm{ms}^{-1}$) are needed in order to obtain multiple equilibria. Moreover, the quasi-geostrophic theory developed in Section 2 is no longer valid since it requires $b = \mathcal{O}(1)$. Charney and DeVore (1979) argue that 5000 km is a typical length scale of blockings. These are persistent anomalies with a barotropic structure, which block the passage of synoptic transient eddies and, consequently, give rise to persistent weather conditions. However, in the spectral model planetary waves must become globally resonant in order to generate a blocking-like structure. This is not in agreement with observations, which show that blockings occur in certain preferent regions and have a local structure. An alternative regional blocking theory for a barotropic atmosphere is developed in Pierrehumbert and Malguzzi (1984).

A more direct testing of the multiple equilibria theory for large scale atmospheric flow was carried out by Charney *et al.* (1981). In this study a barotropic spectral model is considered in a midlatitudinal strip encircling the earth with $N = 35$ and $M = 1$. Here N and M are upper bounds for the zonal and meridional wave-numbers ($|j_1|$) and j_2 of the eigenmodes in (3.10). Its behaviour is studied for parameter values which are thought to be realistic for the atmosphere. As a result, five equilibria are found, some being stable or only weakly unstable. The corresponding flow patterns resemble large-scale preference states of the atmospheric circulation. However, a shortcoming of this model is the absence of wave-triad interactions, since only one meridional wavenumber is included.

Davey (1980) was the first to discuss the relevance of the triad mechanism. He compared results of a nonlinear spectral model ($N = 8$, $M = 4$) with those of a quasi-linear theory, in which wave triads are neglected. He obtained reasonable agreement as long as the driving Rossby number is much smaller than its critical value for which topographic resonance occurs. However, this condition is not generally satisfied: in Källén (1982) a three-component spherical barotropic spectral model is compared with a high-resolution model. One of the conclusions is that the lack of wave triads is a serious shortcoming of the low-order model.

More recently, Tung and Rosenthal (1985) extended the work of Charney *et al.* (1981) using a full nonlinear model (up to $N = 30$, $M = 80$). Using identical parameter values, they did not find multiple equilibria. Therefore, they argue that the relevance of multiple equilibria theory may have been somewhat overestimated, see also Källén (1985). In the first instance this conclusion seems to be in contradiction with the study of Legras and Ghil (1985), where multiple equilibra are obtained in a 25-component model for a large range of parameter values. According to Tung and Rosenthal (1985), this can be a consequence of the different types of forcing used. In their model, as well as in Charney *et al.* (1981), the forcing streamfunction is given as $\psi^*(y) = -U^* y$, where U^* is a

constant zonal velocity. This acts only as a source of momentum and not as a source of vorticity. Actually, the latter type of forcing seems to broaden the region for which multiple equilibria are found.

The model of Charney and DeVore (1979) does not describe internally generated transitions between different weather regimes. An index cycle is only found by adding stochastic perturbations to the equations or by allowing for quasi-statically varying parameters. Therefore, these authors conclude that more modes should be included in the spectral expansions in order to obtain vacillation behaviour. This hypothesis is indeed confirmed by the experiments of Legras and Ghil (1985) and De Swart (1987b). It appears that trajectories in these models can visit alternately three preferent regions in phase space, which are related to a high index, low index, and transitional state. As shown by De Swart (1987b), a barotropic spectral model requires a specific minimum of included modes in the spectral expansions in order to obtain vacillation behaviour. It is also argued that the effects of higher-order transient eddies on the planetary scale flow is very complicated. Although the synoptic forcing terms have a stochastic nature, they are difficult to parameterize, which is in agreement with the results of Kottalam *et al.* (1987).

A general and serious shortcoming of barotropic spectral models is that effects of topographic forcing are over-estimated. In practice, it seems to be no more than a triggering mechanism to generate quasi-stationary waves, as discussed in Section 5.4. Two-level baroclinic spectral models seem to give better results at this point. Again multiple equilibria are found in low-order systems but, although the low-index equilibria cannot exist without topography, their energy is extracted from the potential energy of the mean flow and not from a kinetic energy transfer via the mountain torque (Charney and Straus, 1980). The presence of the baroclinic instability mechanism causes the equilibria to be less stable than in barotropic models and vacillation behaviour is easily produced. However, in the present models, unrealistically large thermal differences between the side-walls of the channel are required to generate index cycles. This is probably related to the fact that the two-level model still has a poor vertical resolution. It can only represent a three-dimensional baroclinic atmosphere with constant vertical shear. A better description is expected from multi-level high resolution spectral models.

So far it seems that the 20-component spectral model of Reinhold and Pierrehumbert (1982) is the simplest model containing all basic physical mechanisms. It allows for the presence of topographic, barotropic, and baroclinic instability mechanisms as well as the occurrence of wave-triad interactions. In this model, a clear distinction appears between a quasi-stationary planetary scale and a transient synoptic scale, see also De Swart (1987b). The system irregularly vacillates between two preference regions in phase space which are situated in the neighbourhood of stationary points of the model. In this paper, a third regime is defined being a transitional type, with residence times much smaller than those

of the two other regimes but much larger than the characteristic time scale of the system. Since qualitatively similar results are obtained with many other spectral models this suggests that the atmosphere has a bimodal character. For a long time this conclusion could not be confirmed by systematic observational data analyses, but recently there are indeed indications of this bimodality, see Benzi *et al.* (1986).

The main conclusion of Reinhold and Pierrehumbert (1982) is that the periods of quasi-stationary behaviour in the large scales are integrally associated with an organized behaviour of the synoptic scales. In other words, if the system is in a certain weather regime, the net forcing of the transients will act to stabilize the large-scale wave structure. However, from time to time perturbations are no longer compensated for and an internal transition to another weather regime will occur. The model seems to reflect many features of the atmospheric circulation as follows from a comparison with the observational results of Dole and Gordon (1983). A problem is that the characteristic residence times of the system in the weather regimes are much larger than those observed in the atmosphere. This is probably due to the severe horizontal and vertical resolution of the model. The question of whether the atmospheric circulation can be described by the internal dynamics of high resolution spectral models only is doubtful. Bruns (1985) and Kruse and Hasselman (1986) argue that such models can only account for part of the observed long-term variability of the atmosphere. They conclude that for a realistic description, stochastic forcing terms should be added to the equations. Using atmospheric data, Egger and Schilling (1983) and Barnett and Roads (1986) have shown that the forcing of planetary scale flow by transient eddies can be modelled as stationary stochastic processes of the red-noise type.

In conclusion we think it is useful to study both deterministic and stochastic spectral models for various horizontal and vertical truncation numbers. The mathematical analysis of deterministic systems can give insight into the qualitative dynamics of the model, such as the existence of preference regions in phase space and transitions of the system between these regions. Clearly, by combining physical intuition and modern mathematical techniques, it is possible to enlarge our knowledge of the dynamics of the atmospheric circulation.

Acknowledgements

These investigations were supported by the Netherlands Foundations for the Technical Sciences (STW), future Science Branch of the Netherlands Organization for the Advancements of Pure Research (ZWO).

I would like to thank J. Grasman, J. D. Opsteegh, and J. T. F. Zimmerman for stimulating comments on an earlier draft.

Appendix A: Spectral Equations of the Two-Level Quasi-geostrophic Model

Consider Equations (3.5) on a two-dimensional domain Ω with boundary conditions and apply the spectral method. We introduce the expansions

$$(\psi, \tau, \psi^*, \tau^*, h) = \sum_{\mathbf{j}} (\psi_{\mathbf{j}}, \tau_{\mathbf{j}}, \psi^*_{\mathbf{j}}, \tau^*_{\mathbf{j}}, h_{\mathbf{j}})\,\phi_{\mathbf{j}}, \tag{A1}$$

where the eigenfunctions $\phi_{\mathbf{j}}$ satisfy (2.21) and the boundary conditions. Substituting (A1) in (3.5) we obtain

$$\lambda^2_{\mathbf{j}}\dot{\psi}_{\mathbf{j}} = \frac{1}{2}\sum_{\mathbf{l}}\sum_{\mathbf{m}} c_{\mathbf{jlm}}(\lambda^2_{\mathbf{l}} - \lambda^2_{\mathbf{m}})(\psi_{\mathbf{l}}\psi_{\mathbf{m}} + \tau_{\mathbf{l}}\tau_{\mathbf{m}}) + \gamma\sum_{\mathbf{l}}\sum_{\mathbf{m}} c_{\mathbf{jlm}}h_{\mathbf{m}}(\psi_{\mathbf{l}} - \tau_{\mathbf{l}}) +$$

$$+\sum_{\mathbf{l}} b_{\mathbf{jl}}\psi_{\mathbf{l}} - C\lambda^2_{\mathbf{j}}(\psi_{\mathbf{j}} - \tau_{\mathbf{j}} - \psi^*_{\mathbf{j}}), \tag{A2a}$$

$$(\lambda^2_{\mathbf{j}} + F')\dot{\tau}_{\mathbf{j}} = \frac{1}{2}\sum_{\mathbf{l}}\sum_{\mathbf{m}} c_{\mathbf{jlm}}[(\lambda^2_{\mathbf{l}} - \lambda^2_{\mathbf{m}} - F')\psi_{\mathbf{l}}\tau_{\mathbf{m}} + (\lambda^2_{\mathbf{l}} - \lambda^2_{\mathbf{m}} + F')\psi_{\mathbf{m}}\tau_{\mathbf{l}}] +$$

$$-\gamma\sum_{\mathbf{l}}\sum_{\mathbf{m}} c_{\mathbf{jlm}}h_{\mathbf{m}}(\psi_{\mathbf{l}} - \tau_{\mathbf{l}}) + \sum_{\mathbf{l}} b_{\mathbf{jl}}\tau_{\mathbf{l}} + C\lambda^2_{\mathbf{j}}(\psi_{\mathbf{j}} - \tau_{\mathbf{j}} - \psi^*_{\mathbf{j}}) +$$

$$+ aF'(\tau^*_{\mathbf{j}} - \tau_{\mathbf{j}}) - 2C'\lambda^2_{\mathbf{j}}\tau_{\mathbf{j}}, \tag{A2b}$$

where

$$c_{\mathbf{jlm}} = \langle \phi_{\mathbf{j}}, J(\phi_{\mathbf{l}}, \phi_{\mathbf{m}})\rangle; \qquad b_{\mathbf{jl}} = \langle \phi_{\mathbf{j}}, J(\phi_{\mathbf{l}}, f)\rangle. \tag{A3}$$

Here

$$\langle A, B\rangle = \int_\Omega AB^{cc}\,\mathrm{d}\mathbf{r} \Big/ \int_\Omega \mathrm{d}\mathbf{r} \tag{A4}$$

defines an inproduct on Ω with cc denoting a complex conjugate. Thus an orthonormalized eigenfunction has a norm, averaged the domain, which equals 1. The interaction coefficients of (A3) obey the relations

$$c_{\mathbf{jlm}} = c_{\mathbf{lmj}},\ c_{\mathbf{jlm}} = -c_{\mathbf{jml}},\ b_{\mathbf{jl}} = -b_{\mathbf{lj}}. \tag{A5}$$

The second one has been used in the derivation of (A2).

Appendix B: Interaction Coefficients for the Eigenfunctions (3.10a)–(3.10b)

Substitution of (3.10a)–(3.10b) in (A3) of Appendix A gives

$$c_{\mathbf{jlm}} = 0, \tag{B1}$$

except for

(A) $\mathbf{j} = (0, j_2)$, $\mathbf{l} = (l_1, l_2)$, $\mathbf{m} = (-l_1, m_2)$; $j_2 + l_2 + m_2$ odd, then

$$\begin{aligned} c_{\mathbf{jlm}} = \frac{i\sqrt{2}\,l_1 b}{\pi} \Bigg\{ (l_2 + m_2)\left[\frac{1}{j_2 + l_2 + m_2} - \frac{1}{j_2 - l_2 - m_2}\right] + \\ - (l_2 - m_2)\left[\frac{1}{j_2 + l_2 - m_2} - \frac{1}{j_2 - l_2 + m_2}\right]\Bigg\}, \end{aligned} \tag{B2}$$

(B) $\mathbf{j} = (j_1, j_2)$, $\mathbf{l} = (l_1, l_2)$, $\mathbf{m} = (m_1, m_2)$, $j_1 + l_1 + m_1 = 0$, $j_2 \pm l_2 \pm m_2 = 0$, then

$$c_{\mathbf{jlm}} = \begin{cases} \dfrac{ib}{\sqrt{2}}(l_1 m_2 - l_2 m_1) & \text{if } j_2 = l_2 + m_2, \\ \dfrac{ib}{\sqrt{2}}(l_1 m_2 + l_2 m_1) & \text{if } j_2 = l_2 - m_2, \\ \dfrac{-ib}{\sqrt{2}}(l_1 m_2 + l_2 m_1) & \text{if } j_2 = -l_2 + m_2. \end{cases} \tag{B3}$$

Furthermore

$$b_{\mathbf{jl}} = 0, \tag{B4}$$

except for $\mathbf{j} = (j_1, j_2)$, $\mathbf{l} = (l_1, l_2)$ with $j_1 + l_1 = 0$, $j_2 = l_2$, then

$$b_{\mathbf{jl}} = i\beta b l_1, \tag{B5}$$

where β is defined in (2.11). Also coefficients which follow from (B2), (B3) and (B5) by permutations of the indices **j**, **l** and **m** are nonzero, see (A5).

Appendix C: Equations of the Twenty-Coefficient Model

$$
\begin{array}{lllll}
(0,1): & \dot{x}_1 = & & \gamma^*_{11}(x_3 - y_3) & - C(x_1 - x^*_1 - y_1) \\
(1,1) & \dot{x}_2 = & -\alpha_{11}(x_1x_3 + y_1y_3) + \beta_{11}x_3 & & - C(x_2 - y_2) \\
 & \dot{x}_3 = & \alpha_{11}(x_1x_2 + y_1y_2) - \beta_{11}x_2 & -\gamma^*_{11}(x_1 - y_1) & - C(x_3 - y_3) \\
(0,2): & \dot{x}_4 = & & \gamma^*_{12}(x_6 - y_6) & - C(x_4 - x^*_4 - y_4) \\
 & \dot{x}_5 = & -\alpha_{12}(x_1x_6 + y_1y_6) + \beta_{12}x_6 & & - C(x_5 - y_5) \\
(1,2): & \dot{x}_6 = & \alpha_{12}(x_1x_5 + y_1y_5) - \beta_{12}x_5 & -\gamma_{12}(x_4 - y_4) & - C(x_6 - y_6) \\
(2,1) & \dot{x}_7 = & -\alpha_{21}(x_1x_8 + y_1y_8) + \beta_{21}x_8 & & - C(x_7 - y_7) \\
 & \dot{x}_8 = & \alpha_{21}(x_1x_7 + y_1y_7) - \beta_{21}x_7 & & - C(x_8 - y_8) \\
(2,2) & \dot{x}_9 = & -\alpha_{22}(x_1x_{10} + y_1y_{10}) + \beta_{22}x_{10} & & - C(x_9 - y_9) \\
 & \dot{x}_{10} = & \alpha_{22}(x_1x_9 + y_1y_9) - \beta_{22}x_9 & & - C(x_{10} - y_{10})
\end{array}
$$

$$
\begin{array}{lllll}
(0,1): & \sigma_{01}\dot{y}_1 = & \frac{5}{6}\epsilon_1(x_2y_3 - x_3y_2) & -\sigma_0\gamma^*_{11}(x_3 - y_3) + ay^*_1 & - C_{01}y_1 + \sigma_0 C(x_1 - x^*_1 \\
(1,1) & \sigma_{11}\dot{y}_2 = & -\alpha'_{11}(\mu_1x_1y_3 + \nu_1x_3y_1) + \sigma_0\beta_{11}y_3 & & - C_{11}y_2 + \sigma_0 Cx_2 \\
 & \sigma_{11}\dot{y}_3 = & \alpha'_{11}(\mu_1x_1y_2 + \nu_1x_2y_1) - \sigma_0\beta_{11}y_2 & +\sigma_0\gamma_{11}(x_1 - y_1) & - C_{11}y_3 + \sigma_0 Cx_3 \\
(0,2): & \sigma_{02}\dot{y}_4 = & & -\sigma_0\gamma^*_{12}(x_6 - y_6) + ay^*_4 & - C_{02}y_4 + \sigma_0 C(x_4 - x^*_4 \\
(1,2): & \sigma_{12}\dot{y}_5 = & -\alpha'_{12}(\mu_4x_1y_6 + \nu_4x_6y_1) + \sigma_0\beta_{12}y_6 & & - C_{12}y_5 + \sigma_0 Cx_5 \\
 & \sigma_{12}\dot{y}_6 = & \alpha'_{12}(\mu_4x_1y_5 + \nu_4x_5y_1) - \sigma_0\beta_{12}y_5 & +\sigma_0\gamma_{12}(x_4 - y_4) & - C_{12}y_6 + \sigma_0 Cx_6 \\
(2,1): & \sigma_{21}\dot{y}_7 = & -\alpha'_{21}(\mu_7x_1y_8 + \nu_7x_8y_1) + \sigma_0\beta_{21}y_8 & & - C_{21}y_7 + \sigma_0 Cx_7 \\
 & \sigma_{21}\dot{y}_8 = & \alpha'_{21}(\mu_7x_1y_7 + \nu_7x_7y_1) - \sigma_0\beta_{21}y_7 & & - C_{21}y_8 + \sigma_0 Cx_8 \\
(2,2): & \sigma_{22}\dot{y}_9 = & -\alpha'_{22}(\mu_8x_1y_{10} + \nu_8x_{10}y_1) + \sigma_0\beta_{22}y_{10} & & - C_{22}y_9 + \sigma_0 Cx_9 \\
 & \sigma_{22}\dot{y}_{10} = & \alpha'_{22}(\mu_8x_1y_9 + \nu_8x_9y_1) - \sigma_0\beta_{22}y_9 & & - C_{22}y_{10} + \sigma_0 Cx_{10}
\end{array}
$$

where

$$\alpha_{nm} = \frac{8\sqrt{2}nb}{\pi}\frac{m^2}{4m^2-1}\frac{n^2b^2+(m^2-1)}{n^2b^2+m^2} = \alpha'_{nm}[n^2b^2+(m^2-1)];$$

$$\delta_{nm} = \frac{64\sqrt{2}nb}{15\pi}\frac{n^2b^2-(m^2-1)}{n^2b^2+m^2} = \delta'_{mm}[n^2b^2-(m^2-1)];$$

$$\epsilon_n = \frac{16\sqrt{2}nb}{5\pi};$$

$$\rho_{nm} = \frac{9b}{2}\left[\frac{(n-2)^2b^2-(m-2)^2}{n^2b^2+m^2}\right] = 3\rho'_{nm}[(n-2)^2b^2-(m-2)^2];$$

$$\sigma_{nm} = \sigma_0 + \frac{1}{n^2b^2+m^2};$$

$$\sigma_0 = (F')^{-1}, \qquad \mu_1 = \sigma_0b^2+1, \qquad \mu_2 = 3\sigma_0(b^2-1)+1,$$
$$\mu_6 = 3\sigma_0b^2+1, \qquad \mu_7 = 4\sigma_0b^2+1, \qquad \mu_8 = \sigma_0(4b^2+3)+1.$$

$$+ y_3y_5)] \qquad \text{(C1)}$$

$$- \rho_{11}[(x_5x_8 + y_5y_8) - (x_6x_7 + y_6y_7)] \qquad \text{(C2)}$$

$$+ \rho_{11}[(x_5x_7 + y_5y_7) + (x_6x_8 + y_6y_8)] \qquad \text{(C3)}$$

$$+ \epsilon_2[(x_7x_{10} + y_7y_{10}) - (x_8x_9 + y_8y_9)] \qquad \text{(C4)}$$

$$+ \rho_{12}[(x_2x_8 + y_2y_8) - (x_3x_7 + y_3y_7)] + \gamma'_{12}(x_8 - y_8) \qquad \text{(C5)}$$

$$- \rho_{12}[(x_2x_7 + y_2y_7) + (x_3x_8 + y_3y_8)] - \gamma'_{12}(x_7 - y_7) \qquad \text{(C6)}$$

$$- \rho_{21}[(x_2x_6 + y_2y_6) + (x_3x_5 + y_3y_5)] + \gamma'_{21}(x_6 - y_6) \qquad \text{(C7)}$$

$$+ \rho_{21}[(x_2x_5 + y_2y_5) - (x_3x_6 + y_3y_6)] - \gamma'_{21}(x_5 - y_5) \qquad \text{(C8)}$$

$$\text{(C9)}$$

$$\text{(C10)}$$

$$+ \tfrac{2}{3}\epsilon_1(x_5y_6 - y_6x_5) + \tfrac{5}{6}\epsilon_2(x_7y_8 - x_8y_7) + \tfrac{2}{3}\epsilon_2(x_9y_{10} - x_{10}y_9) \qquad \text{(C11)}$$

$$- \delta'_{11}(\mu_1x_4y_6 + \nu_1x_6y_4) - \rho'_{11}[\mu_2(x_5y_8 - x_6y_7) + \nu_2(x_8y_5 - x_7y_6)] \qquad \text{(C12)}$$

$$+ \delta'_{11}(\mu_1x_4y_5 + \nu_1x_5y_4) + \rho'_{11}[\mu_2(x_5y_7 + x_6y_8) + \nu_2(x_7y_5 + x_8y_6)] \qquad \text{(C13)}$$

$$+ \tfrac{1}{3}\epsilon_1[\mu_3(x_2y_6 - x_3y_5) + \nu_3(x_6y_2 - x_5y_3)] + \tfrac{1}{3}\epsilon_2[\mu_3(x_7y_{10} - x_8y_9) + \nu_3(x_{10}y_7 - x_9y_8)] \qquad \text{(C14)}$$

$$- \delta'_{12}(\mu_5x_4y_3 + \nu_5x_3y_4) + \rho'_{12}[\mu_6(x_2y_8 - x_3y_7) + \nu_6(x_8y_2 - x_7y_3)] - \sigma_0\gamma'_{12}(x_8 - y_8) \qquad \text{(C15)}$$

$$+ \delta'_{12}(\mu_5x_4y_2 + \nu_5x_2y_4) - \rho'_{12}[\mu_6(x_2y_7 + x_3y_8) + \nu_6(x_7y_2 + x_8y_3)] + \sigma_0\gamma'_{12}(x_7 - y_7) \qquad \text{(C16)}$$

$$- \delta'_{21}(\mu_7x_4y_{10} + \nu_7x_{10}y_4) + \rho'_{21}[\mu_3(x_2y_6 + x_3y_5) + \nu_3(x_5y_3 + x_6y_2)] - \sigma_0\gamma'_{21}(x_6 - y_6) \qquad \text{(C17)}$$

$$+ \delta'_{21}(\mu_7x_4y_9 + \nu_7x_9y_4) - \rho'_{21}[\mu_3(x_2y_5 - x_3y_6) + \nu_3(x_5y_2 - x_6y_3)] + \sigma_0\gamma'_{21}(x_5 - y_5) \qquad \text{(C18)}$$

$$- \delta'_{22}(\mu_9x_4y_8 + \nu_9x_8y_4) \qquad \text{(C19)}$$

$$+ \delta'_{22}(\mu_9x_4y_7 + \nu_9x_7y_4) \qquad \text{(C20)}$$

$$\beta_{nm} = \frac{\beta nb}{n^2b^2 + m^2},$$

$$\gamma^*_{nm} = \frac{4m}{4m^2 - 1}\frac{\sqrt{2}nb\gamma}{\pi},$$

$$\gamma_{nm} = \frac{4m^3}{4m^2 - 1}\frac{\sqrt{2}nb\gamma}{\pi(n^2b^2 + m^2)},$$

$$\gamma'_{nm} = \frac{3b\gamma}{4(n^2b^2 + m^2)},$$

$$C_{nm} = \sigma_0(C' + 2C'') + \frac{a}{n^2b^2 + m^2},$$

$\mu_3 = 3\sigma_0 + 1$, $\mu_4 = \sigma_0(b^2 + 3) + 1$, $\mu_5 = \sigma_0(b^2 - 3) + 1$,
$\mu_9 = \sigma_0(4b^2 - 3) + 1$, and $\nu_i = \mu_i - 2 (i = 1, 2, \ldots, 9)$.

References

Baer, F.: Analytical solutions to low-order spectral systems, *Arch. Meteor. Geoph. Biokl.* **A19** (1970), 255–282.

Baer, F.: Energetics of low-order spectral systems, *Tellus* **23** (1971), 218–231.

Barnett, T. P. and Roads, J. O.: Stochastic forcing and prediction of low-frequency planetary scale flow, *J. Atmos. Sci.* **43** (1986), 940–947.

Baur, F., Hess, P., and Nagel, H.: *Kalender der Grosswetterlagen Europas 1881–1939*, Bad Homburg v.d. H., 1944.

Benzi, R., Malguzzi, P., Speranza, A., and Sutera, A.: The statistical properties of the general atmospheric circulation: observational evidence on a minimal theory of bimodality, *Quart. J. R. Meterol. Soc.* **112** (1986), 661–674.

Blackman, M., Madden, R. A., Wallace, J. M., and Gutzler, D. S.: Geographical variations in the vertical structure of geopotential height fluctuations, *J. Atmos. Sci.* **36** (1979), 2450–2466.

Bruns, T.: Contribution of linear and nonlinear processes to the long term variability of large scale atmospheric flow, *J. Atmos. Sci.* **42** (1985), 2506–2522.

Bryan, K.: A numerical investigation of certain features of the general circulation, *Tellus* **11** (1959), 163–174.

Charney, J. G. and DeVore J. G.: Multiple flow equilibria in the atmosphere and blocking, *J. Atmos. Sci.* **36** (1979), 1205–1216.

Charney, J. G. and Straus, D. M.: Form-drag instability, multiple equilibria and propagating planetary waves in baroclinic, orographically forced, planetary wave systems, *J. Atmos. Sci.* **37** (1980), 1157–1176.

Charney, J. G., Shukla, J., and Mo, K. C.: Comparison of a barotropic blocking theory with observation, *J. Atmos. Sci.* **38** (1981), 762–779.

Constantin, P., Foias, C., Manley, O. P., and Temam, R.: Determining modes and fractal dimensions of turbulent flows, *J. Fluid Mech.* **150** (1985), 427–440.

Davey, M. K.: A quasi-linear theory for rotating flow over topography. Part I: steady β-plane channel, *J. Fluid Mech.* **99** (1980), 267–292.

De Swart, H. E.: Analysis of a six component barotropic spectral model: chaotic motion, predictability and vacillation, CWI report AM-R8710 (1987a).

De Swart, H. E.: A study on the relation between predictability and interaction between different scales of motion with a 'minimum order' atmospheric spectral model, CWI report (1987b) to appear.

De Swart, H. E. and Grasman, J.: Sources of stochastic behaviour of dynamical systems, in Proc. Workshop *The Dynamics of Long Waves in the Atmosphere*, Kristineberg, Sweden, 1984, pp. 147–152.

De Swart, H. E. and Grasman, J.: Effect of stochastic perturbations on a low-order spectral model of the atmospheric circulation, *Tellus* **39A**, (1987), 10–24.

Doedel, E. J.: *AUTO 86 User Manual, Software for Continuation and Bifurcation Problems in Ordinary Differential Equations*, Concordia University, Montreal, 1986.

Dole, R. M. and Gordon, N. D.: Persistent anomalies of the extratropical Northern Hemisphere wintertime circulation: geographical distribution and regional persistence characteristics, *Mon. Wea. Rev.* **111** (1983), 1567–1586.

Dutton, J.: The nonlinear quasi-geostrophic equation: existence and uniqueness of solutions on a bounded domain, *J. Atmos. Sci.* **31** (1974), 422–433.

Dutton, J.: The nonlinear quasi-geostrophic equation. Part II: predictability, recurrence and limit properties of thermally forced and unforced flows, *J. Atmos. Sci.* **33** (1976a), 1431–1453.

Dutton, J.: Aperiodic trajectories and stationary points in a three-component spectral model of atmospheric flow, *J. Atmos. Sci.* **33** (1976b), 1499–1504.

Egger, J.: Stochastically driven large-scale circulations with multiple equilibria, *J. Atmos. Sci.* **38** (1981), 2608–2618.

Egger, J. and Schilling, H. D.: On the theory of the long-term variability of the atmosphere, *J. Atmos. Sci.* **40** (1983), 1073–1085.

Fjørtoft, R.: On the changes in the spectral distribution of kinetic energy for two-dimensional, nondivergent flow, *Tellus* **5** (1953), 225–230.

Franceshini, V., Tebaldi, C., and Zironi, F.: Fixed point limit behaviour of N-mode truncated Navier–Stokes equations as N increases, *J. Stat. Phys.* **35** (1983), 387–397.

Frederiksen, J. S.: A unified three-dimensional instability theory of the onset of blocking and cyclogenesis II: teleconnection patterns, *J. Atmos. Sci.* **40** (1983), 2593–2609.

Galin, M. B.: Energetics of a twelve-component model of the general atmospheric circulation, *Atmos. Ocean Phys.* **15** (1979), 89–92.

Galin, M. B. and Kirichkov, S. Ye.: Effect of orography on the nonzonal circulation of the atmosphere and blocking formations, *Atmos. Ocean. Phys.* **21**, (1985), 533–538.

Gill, A. E.: *Atmosphere-Ocean Dynamics*, Academic Press, New York, 1982.

Glendinning, D. and Sparrow, C.: Local and global behaviour near homoclinic orbits, *J. Stat. Phys.* **35**, 645–697.

Gottlieb, D. and Orszag, S. A. *Numerical Analysis of Spectral Methods*, Regional Conference Series in Applied Mathematics 26, SIAM, Philadelphia, 1977.

Grebogi, C., Ott, E., and Yorke, J. A.: Crises, sudden changes in chaotic attractors, and transient chaos, *Physica* **7D** (1986), 181–200.

Guckenheimer, J. and Holmes, P.: *Nonlinear Oscillations, Dynamical Systems and Bifurcation of Vectorfields*, Springer-Verlag, Berlin, 1983.

Hess, P. and Brezowsky, H.: Katalog der Grosswetteranlagen Deutschlands, *Ber. Dtsch. Wetterdienstes* **113** (1969).

Jarraud, M. and Baede, A. P. M.: The use of spectral techniques in numerical weather prediction, *Lect. Appl. Math.* **22** (1985), 1–41.

Källén, E.: The nonlinear effects of orographic and momentum forcing in a low-order, barotropic model, *J. Atmos. Sci.* **38** (1981), 2150–2163.

Källén, E.: Bifurcation properties of quasi-geostrophic, barotropic models and their relation to atmospheric blocking, *Tellus* **34** (1982), 255–265.

Källén, E.: A note on orographically induced instabilities in two-layer models, *J. Atmos. Sci.* **40** (1983), 500–505.

Källén, E.: On hysteresis-like effects in orographically forced models, *Tellus* **37A** (1985), 249–257.

Keller, H. B.: Numerical solution of bifurcation and nonlinear eigenvalue problems, in P. H. Rabinowitz (ed.), *Applications of Bifurcation Theory*, Academic Press, New York, 1977, pp. 359–384.

Kottalam, J., West, B. J., and Lindenberg, K.: Fluctuations and dissipation in multiple flow equilibria, preprint,University of California at San Diego, 1987.

Kruse, H. A. and Hasselman, K.: Investigation of processes governing the large-scale variability of the atmosphere using low-order barotropic spectral models as a statistical tool, *Tellus* **38A** (1986), 12–24.

Kubota, S.: Some characteristics of the barotropic atmosphere with respect to the scales of disturbance, *Papers Meteorol. Geoph. (Tokyo)* **12** (1961), 183–198.

Kubota, S., Hirose, M., Kikuchi, Y., and Kurihara, Y.: Barotropic forecasting with the use of surface spherical harmonic representations, *Papers Meteor Geoph. (Tokyo)* **12** (1961), 199–215.

Legras, B. and Ghil, M.: Persistent anomalies, blocking and variations in atmospheric predictability, *J. Atmos. Sci.* **42** (1985), 433–471.

Lilly, D. K.: On the computational stability of numerical solutions of time-dependent, non-linear geophysical fluid dynamics problems, *Mon. Wea. Rev.* **93**, (1965), 11–26.

Lorenz, E. N.: Maximum simplification of the dynamic equations, *Tellus* **12** (1960), 243–254.

Lorenz, E. N.: Deterministic nonperiodic flow, *J. Atmos. Sci.* **20** (1963a), 130–141.

Lorenz, E. N.: The mechanics of vacillation, *J. Atmos. Sci.* **20** (1963b), 448–464.

Lorenz, E. N.: A study of the predictability of a 28-variable atmospheric model, *Tellus* **17** (1965), 321–333.

Lorenz, E. N.: The predictability of a flow which possesses many scales of motion, *Tellus* **21** (1969), 289–307.

Lorenz, E. N.: Attractor sets and quasi-geostrophic equilibrium, *J. Atmos. Sci.* **37** (1980), 1685–1699.

Lorenz, E. N.: Low-order models of atmospheric circulations, *J. Meteor. Soc. Japan* **60** (1982), 255–267.

Lorenz, E. N.: Irregularity: a fundamental property of the atmosphere, *Tellus* **36A** (1984), 98–110.
Mitchell, K. E. and Dutton, J. A.: Bifurcations from stationary to periodic solutions in a low-order model of forced, dissipative barotropic flow, *J. Atmos. Sci.* **38** (1981), 690–716.
Namias, J.: The index cycle and its role in the general circulation, *J. Meteorol.* **7** (1950), 130–139.
Oerlemans, J.: An objective approach to breaks in the weather, *Mon. Wea. Rev.* **106** (1978), 1672–1679.
Opsteegh, J. D. and Vernekar, A. D. A simulation of the January standing wave pattern including the effect of transient eddies, *J. Atmos. Sci.* **39** (1982), 734–744.
Orszag, S. A.: Transform method for calculation of vector coupled sums. Application to the spectral form of the vorticity equation, *J. Atmos. Sci.* **27** (1970), 890–895.
Pedlosky, J.: *Geophysical Fluid Dynamics*, Springer-Verlag, New York, 1979.
Pedlosky, J.: Resonant topographic waves in barotropic and baroclinic flows, *J. Atmos. Sci.* **38** (1981), 2626–2641.
Phillips, N. A.: Energy transformations and meridional circulations associated with simple baroclinic waves in a two-level, quasi-geostrophic model, *Tellus* **6** (1954), 273–286.
Pierrehumbert, R. T. and Malguzzi, P.: Forced coherent structures and local multiple equilibria in a barotropic atmosphere, *J. Atmos. Sci.* **41** (1984), 246–257.
Platzman, G. W.: The analytical dynamics of the spectral vorticity equation, *J. Atmos. Sci.* **19** (1962), 313–328.
Reinhold, B. B. and Pierrehumbert, R. T.: Dynamics of weather regimes: quasi-stationary waves and blocking, *Mon. Wea. Rev.* **110** (1982), 1105–1145.
Roads, J. O.: Stable near-resonant states forced by orography in a simple baroclinic model, *J. Atmos. Sci.* **37** (1980), 2381–2395.
Roads, J. O.: Stable and unstable near-resonant states in multilevel, severely truncated, quasi-geostrophic models, *J. Atmos. Sci.* **39** (1982), 203–224.
Saltzman, B.: On the maintenance of the large-scale quasi-permanent disturbances of the atmosphere, *Tellus* **11** (1959), 425–431.
Shirer, H. N. and Wells, R.: *Mathematical Structure of the Singularities at the Transitions between Steady States in Hydrodynamic Systems*, Springer-Verlag, Berlin, 1983.
Silberman, I.: Planetary waves in the atmosphere, *J. Meteor.* **11** (1954), 27–34.
Silnikov, L. P.: A case of the existence of a denumerable set of periodic motions, *Sov. Math. Dokl.* **36** (1965), 163–166.
Thompson, J. M. T. and Stewart, H. B.: *Nonlinear Dynamics and Chaos*, Wiley, Chichester, 1986.
Tung, K. K. and Rosenthal, A. J.: Theories of multiple equilibria—a critical reexamination. Part I: barotropic models, *J. Atmos. Sci.* **42** (1985), 2804–2819.
Voigt, R. G., Gottlieb, D., and Yousoff Hussaini, M. (eds.): *Spectral Methods for Partial Differential Equations*, SIAM, Philadelphia, 1984.
Vickroy, J. G. and Dutton, J. A.: Bifurcation and catastrophe in a simple, forced, dissipative quasi-geostrophic flow, *J. Atmos. Sci.* **36** (1979), 42–52.
Wiin-Nielsen, A.: Steady states and stability properties of a low-order barotropic system with forcing and dissipation, *Tellus* **31** (1979), 375–386.
Wiin-Nielsen, A.: Low- and high-index steady states in a low-order model with vorticity forcing, *Contr. Atmos. Phys.* **57** (1984), 291–306.
Wolf, A., Swift, J. B., Swinney, H. L., and Vastano, J. A.: Determining Lyapunov exponents from a time series, *Physica* **6D** (1985), 285–317.
Yao, M. S.: Maintenance of quasi-stationary waves in a two-level quasi-geostrophic spectral model with topography, *J. Atmos Sci.* **37** (1980), 29–43.
Yoden, S.: Nonlinear interactions in a two-layer, quasi-geostrophic, low-order model with topography. Part I: zonal flow-forced wave interactions, *J. Meteorol. Soc. Japan* **61** (1983a), 1–18.
Yoden, S.: Nonlinear interactions in a two-layer, quasi-geostrophic, low-order model with topography. Part II: interactions between zonal flow, forced waves and free waves, *J. Meterol. Soc. Japan* **61** (1983b), 19–35.
Yoden, S.: Bifurcation properties of a quasi-geostrophic, barotropic, low-order model with topography, *J. Metorol. Soc. Japan* **63** (1985), 535–546.
Yoden, S. and Mukougawa, H.: Instabilities of a baroclinic zonal flow in the presence of surface topography, *J. Meteorol. Soc. Japan* **61** (1983), 789–804.